Population Models of Epidemics with Infection Age and Vaccination Age Structure

Glenn Webb * and Xinyue Zhao *

Posted Date: 27 November 2023

doi: 10.20944/preprints202311.1686.v1

Keywords: Keywords: COVID-19; data; transmission; asymptomatic

Article

Population Models of Epidemics with Infection Age and Vaccination Age Structure

Glenn Webb [1,*] and Xinyue Evelyn Zhao [2,*]

[1] Department of Mathematics, Vanderbilt University, Nashville, TN 37240, USA
[2] Department of Mathematics, University of Tennessee, Knoxville, TN 37996, USA
* glenn.f.webb@vanderbilt.edu (G.W.); xzhao45@utk.edu (X.E.Z.)

Abstract: A population dynamics epidemic model is developed that incorporates age of infection and age of vaccination. The model analyzes pre-symptomatic and symptomatic periods of an infected individual in terms of infection age. The model analyzes the efficacy of vaccination in terms of vaccination age. The model is applied to the 2003 SARS epidemic in Taiwan and the current COVID-19 epidemic in New York State.

Keywords: COVID-19; data; transmission; asymptomatic; symptomatic; vaccination

1. Introduction

The objective of this work is to model the effects of quarantine, vaccination, and hospital isolation on the transmission of infection in an epidemic population. The focus of the model is on the infectious and symptomatic periods of an infective, which may or may not overlap. For a viral respiratory disease with severe morbidity and mortality, the symptomatic period typically results in hospital isolation as soon as the disease is recognized as a major public health problem. If the infectious and symptomatic periods coincide, or if the infectious period follows the appearance of symptoms, then the hospitalization of symptomatic patients is effective isolation of infectious individuals. If, however, the infectious period precedes the symptomatic phase, then there is much greater potential for disease transmission to susceptibles. The efficacy of vaccination during the epidemic is incorporated into the model, to account for the acquisition of immunity over a time period of vaccinated individuals.

The model is applicable to influenza epidemics such as the SARS epidemic of 2003 and the current COVID-19 pandemic. The 2003 SARS epidemic was contained, in part, because SARS infectives were infectious after manifesting symptoms, which allowed their identification and controlled isolation in hospitals. Vaccination has played a key role in the containment of the current COVID-19 pandemic. The central point of the study here is that in a future epidemic comparable to the 2003 SARS epidemic and the current COVID-19 pandemic, quarantine, vaccination, and hospitalization (isolation) will be critical elements of containment.

There is an extensive literature of works involving epidemic dynamics and vaccination implementations. In our *References*, we have listed many of these works.

The organization of this paper is as follows: In Section 2 we present the compartments and parameters of the model. In Section 3 we present the equations of the model. In Section 4 we analyze the model. In Section 5 we apply the model to the 2003 SARS epidemic in Taiwan. In Section 6 we apply the model to the COVID-19 epidemic in New York State. In Section 7, we provide a discussion of our results and highlight some future work.

2. Materials and Methods

The compartments of the model are susceptibles (S), vaccinated (V), exposed infectives (E), infectious infectives (I), hospitalized infectives (H) (including mortality), quarantined infectives (Q), and recovered infectives (R) (see Figure 1). The key features of this model are (1) infected individuals are tracked by disease age a_i, and the incubation, infectious, and symptomatic stages of the disease are modeled by the disease age of the infected individual, and (2) vaccinated individuals are tracked

Preprints (www.preprints.org) | NOT PEER-REVIEWED | Posted: 27 November 2023 doi:10.20944/preprints202311.1686.v1

by vaccination age a_v, and their susceptibility to infection depends on their vaccination age as they gradually acquire and lose immunity.

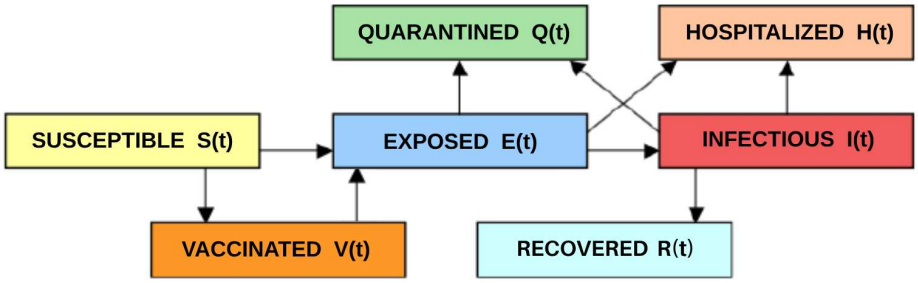

Figure 1. Diagram of susceptible, vaccinated, exposed, infectious, hospitalized, quarantined, and recovered compartments of the model.

The infected population has infection age density $i(a_i, t)$. Infectives begin the disease course at age $a_i = 0$, are infected but noninfectious (exposed) from age $a_i = 0$ to age $a_i = r$, and infectious from age $a_i = r$ to age $a_i = r + s$. Infectives are no longer infectious after reaching the disease age $a_i = r + s$ and are considered recovered, with the assumption that they cannot be re-infected. Thus,

$$E(t) = \int_0^r i(a_i, t)da_i, \tag{1}$$

$$I(t) = \int_r^{r+s} i(a_i, t)da_i, \tag{2}$$

$$R(t) = \int_0^t i(r + s, \hat{t})d\hat{t}, t \geq 0. \tag{3}$$

Infectives with infection age $a_i \leq r + s$ can be removed from the exposed class $E(t)$ or the infectious class $I(t)$ at time t due to hospitalization or quarantine. Mortality due to the disease is included in the hospitalized compartment. Transmission of infection to susceptibles, hospitalization, manifestation of symptoms, and quarantine all depends on disease age. It is also assumed that hospitalized, quarantined, and recovered infectives do not transmit the disease to susceptibles.

The vaccinated population has vaccination age density $v(a_v, t)$. Vaccinated individuals begin with vaccination age $a_v = 0$ and then have increasing or decreasing immunity to infection as their vaccination age a_v increases over time. We assume there are no vaccinated individuals at $t = 0$, and the vaccination starts on or after $t = 0$, thus $a_v \leq t$. The number of vaccinated individuals at time t is

$$V(t) = \int_0^t v(a_v, t)da_v. \tag{4}$$

The population of vaccinated individuals has a gain from the susceptible class and a loss to the infected class, since vaccination efficacy is incomplete.

The model does not take into account demographics (births and deaths) of the population. The time scale of the model (the units of t are typically days) is comparable to a small fraction of the lifespan of individuals in the population. The asymptotic behavior of the model populations, corresponding to large time, is comparable to a small fraction of the typical lifespan of individuals. For human populations, the typical time units are days and the meaningful time scale of the model is several years.

The parameters of the model are as follows: $\alpha(a_i)$ is the disease transmission rate from an infectious individual with infection age a_i to a susceptible individual, ν is the rate of vaccination of susceptibles, 1-$\sigma(a_v)$ is the effectiveness of vaccination for a vaccinated individual with vaccination

Preprints (www.preprints.org) | NOT PEER-REVIEWED | Posted: 27 November 2023 doi:10.20944/preprints202311.1686.v1

age a_v, $\beta_H(a_i)$ is the transition rate of infectives with infection age a_i to hospitalization and $\beta_Q(a_i)$ is the transition rate of infectives with infection age a_i to quarantine.

2.1. Equations of the Model

The equations of the model are as follows: for $t \geq 0$,

$$\frac{d}{dt}S(t) = -\left(\int_r^{r+s} \alpha(a_i)i(a_i,t)da_i + \nu\right)S(t), \tag{5}$$

$$\frac{\partial}{\partial t}i(a_i,t) + \frac{\partial}{\partial a_i}i(a_i,t) = -\Big(\beta_H(a_i) + \beta_Q(a_i)\Big)i(a_i,t), 0 \leq a_i \leq r+s, \tag{6}$$

$$i(0,t) = \int_r^{r+s} \alpha(a_i)i(a_i,t)da_i \left(S(t) + \int_0^t \sigma(a_v)v(a_v,t)da_v\right), \tag{7}$$

$$\frac{\partial}{\partial t}v(a_v,t) + \frac{\partial}{\partial a_v}v(a_v,t) = -\sigma(a_v)\left(\int_r^{r+s} \alpha(a_i)i(a_i,t)da_i\right)v(a_v,t), 0 \leq a_v \leq t, \tag{8}$$

$$v(0,t) = \nu S(t), \tag{9}$$

with initial conditions

$$S(0) = S_0, i(a_i,0) = i_0(a_i), v(a_v,0) = v_0(a_v) \equiv 0. \tag{10}$$

(we assume there are no vaccinated individuals at $t = 0$).

2.2. Analysis of the Model

Assume the following hypothesis: $\nu \geq 0, \alpha$ is nonnegative and piecewise continuous on $[r, r+s)$, β_H and β_Q are nonnegative and piecewise continuous on $[0, r+s)$, σ is nonnegative and piecewise continuous on $[0,\infty)$, $S_0 > 0$, i_0 is nonnegative and piecewise continuous on $[0, r+s)$, and $v_0 \equiv 0$ on $[0,\infty)$. The existence of unique nonnegative solutions in $[0,\infty) \times L^1[0, r+s) \times L^1[0,\infty)$ to the system of equations (3.1) - (3.5), with initial conditions (3.11), can be proven with the techniques developed in [1]. The asymptotic behavior of this system without vaccination is investigated in [2,3]. We prove the following asymptotic behavior of the solutions with vaccination:

Theorem 1. *Assume that for* $0 \leq a_i \leq r+s$, $\beta_H(a_i) + \beta_Q(a_i) \geq \bar{\beta} > 0$, $0 \leq \alpha(a_i) \leq \bar{\alpha} > 0$, *and* $0 \leq \sigma(a_i) \leq \bar{\sigma} > 0$. *The solutions of (3.1) - (3.5) with initial conditions (3.11) have the following asymptotic behavior:*

$$\lim_{t\to\infty} S(t) = S_\infty \geq 0, \lim_{t\to\infty} E(t) = 0, \lim_{t\to\infty} I(t) = 0. \tag{11}$$

If $\nu > 0$ *(vaccination), then* $S_\infty = 0$. *If* $\nu = 0$ *(no vaccination), then* S_∞ *satisfies*

$$S_\infty = exp\Big[-\Big(\Gamma + (S(0) - S_\infty)\Lambda\Big)\Big]S(0), \tag{12}$$

where

$$\Gamma = \int_r^{r+s} \alpha(a_i) \int_0^{a_i} i_0(u) exp\Big[-\int_u^{a_i}(\beta_H(b) + \beta_Q(b))db\Big]duda_i, \tag{13}$$

$$\Lambda = \int_r^{r+s} \alpha(a_i) exp\Big[-\int_0^{a_i}(\beta_H(b) + \beta_Q(b))db\Big]da_i. \tag{14}$$

Preprints (www.preprints.org) | NOT PEER-REVIEWED | Posted: 27 November 2023 doi:10.20944/preprints202311.1686.v1

Proof. Let $\beta(a_i) = \beta_H(a_i) + \beta_H(a_i) \geq \bar{\beta} > 0, 0 \leq a_i \leq r+s$. We first prove (11). From (5) for $t \geq 0$

$$S(t) = \exp(-\nu t) exp\left[-\int_0^t \left(\int_r^{r+s} \alpha(a_i) i(a_i, \hat{t}) da_i \right) d\hat{t} \right] S(0) \tag{15}$$

Then, it implies that $S(t)$ is non-increasing and $S_\infty = \lim_{t\to\infty} S(t) \geq 0$. It is also clear that $S_\infty = 0$ if $\nu > 0$. In addition, by evaluating the integral of (5) from 0 to t, we have

$$S(t) - S(0) = -\int_0^t \left(\int_r^{r+s} \alpha(a_i) i(a_i, \hat{t}) da_i \right) S(\hat{t}) d\hat{t} - \nu \int_0^t S(\hat{t}) d\hat{t},$$

which is equivalent to

$$S(t) + \int_0^t \left(\int_r^{r+s} \alpha(a_i) i(a_i, \hat{t}) da_i \right) S(\hat{t}) d\hat{t} = S(0) - \nu \int_0^t S(\hat{t}) d\hat{t}. \tag{16}$$

We then derive equations for $V(t)$. Combining (4), (8), and (9), we obtain, for $t \geq 0$,

$$\begin{aligned} V'(t) &= \frac{d}{dt}\left(\int_0^t v(a_v, t) da_v \right) = v(t,t) + \int_0^t v_t(a_v, t) da_v \\ &= v(t,t) + \int_0^t \left[-v_{a_v}(a_v, t) - \sigma(a_v) \left(\int_r^{r+s} \alpha(a_i) i(a_i, t) d_{a_i} \right) v(a_v, t) \right] da_v \\ &= v(t,t) - v(t,t) + v(0,t) - \int_0^t \sigma(a_v) \left(\int_r^{r+s} \alpha(a_i) i(a_i, t) d_{a_i} \right) v(a_v, t) da_v \\ &= \nu S(t) - \int_0^t \left(\int_r^{r+s} \alpha(a_i) i(a_i, t) d_{a_i} \right) \sigma(a_v) v(a_v, t) da_v, \end{aligned}$$

which integrates to

$$\begin{aligned} V(t) + \int_0^t \left(\int_0^{\hat{t}} \left[\left(\int_r^{r+s} \alpha(a_i) i(a_i, \hat{t}) da_i \right) \sigma(a_v) v(a_v, \hat{t}) \right] da_v \right) d\hat{t} \\ = V(0) + \int_0^t \nu S(\hat{t}) d\hat{t}. \end{aligned} \tag{17}$$

Then (15), (17), and the nonnegativity of solutions imply $\lim_{t\to\infty} V(t)$ exists. Next, we consider $E(t)$ and $I(t)$. Using equations (1), (2), and (6), we have, for $t \geq 0$,

$$\begin{aligned} E'(t) &= \frac{d}{dt}\left(\int_0^r i(a_i, t) da_i \right) = \int_0^r i_t(a_i, t) da_i = \int_0^r \left(-i_{a_i}(a_i, t) - \beta(a_i) i(a_i, t) \right) da_i \\ &= i(0,t) - i(r,t) - \int_0^r \beta(a_i) i(a_i, t) da_i, \end{aligned} \tag{18}$$

$$\begin{aligned} I'(t) &= \frac{d}{dt}\left(\int_r^{r+s} i(a_i, t) da_i \right) = \int_r^{r+s} i_t(a_i, t) da_i = \int_r^{r+s} \left(-i_{a_i}(a_i, t) - \beta(a_i) i(a_i, t) \right) da_i \\ &= i(r,t) - i(r+s,t) - \int_r^{r+s} \beta(a_i) i(a_i, t) da_i, \end{aligned} \tag{19}$$

where the boundary condition $i(0,t)$ is defined in (7). Adding up these two equations gives

$$E'(t) + I'(t) = i(0,t) - i(r+s,t) - \int_0^{r+s} \beta(a_i) i(a_i, t) da_i,$$

Preprints (www.preprints.org) | NOT PEER-REVIEWED | Posted: 27 November 2023 doi:10.20944/preprints202311.1686.v1

which integrates to

$$E(t) + I(t) = E(0) + I(0) + \int_0^t \left(i(0,\hat{t}) - i(r+s,\hat{t}) - \int_0^{r+s} \beta(a_i) i(a_i,\hat{t}) da_i \right) d\hat{t}. \tag{20}$$

In equation (20), we use (7) to derive

$$\begin{aligned}
\int_0^t i(0,\hat{t}) &= \int_0^t \int_r^{r+s} \alpha(a_i) i(a_i,\hat{t}) da_i \left(S(\hat{t}) + \int_0^{\hat{t}} \sigma(a_v) v(a_v,\hat{t}) da_v \right) d\hat{t} \\
&= \int_0^t \left(\int_r^{r+s} \alpha(a_i) i(a_i,\hat{t}) da_i \right) S(\hat{t}) d\hat{t} \\
&\quad + \int_0^t \left(\int_r^{r+s} \alpha(a_i) i(a_i,\hat{t}) da_i \right) \left(\int_0^{\hat{t}} \sigma(a_v) v(a_v,\hat{t}) da_v \right) d\hat{t} \\
&= \int_0^t \left(\int_r^{r+s} \alpha(a_i) i(a_i,\hat{t}) da_i \right) S(\hat{t}) d\hat{t} \\
&\quad + \int_0^t \left(\int_0^{\hat{t}} \left[\left(\int_r^{r+s} \alpha(a_i) i(a_i,\hat{t}) da_i \right) \sigma(a_v) v(a_v,\hat{t}) \right] da_v \right) d\hat{t}.
\end{aligned} \tag{21}$$

We observe that the first term in (21) is equal to the second term in the left-hand side of (16), and the second term in (21) equals the second term in the left-hand side of (17). Therefore, when summing up equations (16), (17), (20), we find that the two terms in (21) cancel out. Consequently, for $t \geq 0$, we have,

$$\begin{aligned}
&S(t) + V(t) + E(t) + I(t) + \int_0^t i(r+s,\hat{t}) d\hat{t} + \int_0^t \left(\int_0^{r+s} \beta(a_i) i(a_i,\hat{t}) da_i \right) d\hat{t} \\
&\quad = S(0) + V(0) + E(0) + I(0)
\end{aligned} \tag{22}$$

Since $\beta(a_i) \geq \bar{\beta}$ for $0 \leq a_i \leq r+s$, (22) implies

$$\int_0^\infty \left(E(t) + I(t) \right) dt < \infty. \tag{23}$$

Thus, (15), (17), (22), and (23) imply

$$\lim_{t\to\infty} E(t) = \lim_{t\to\infty} I(t) = 0.$$

Lastly, we prove that if $\nu = 0$ (no vaccination), then $S_\infty > 0$ and satisfies (12). From (6)

$$i(a_i,t) = \begin{cases} i_0(a_i - t) exp[-\int_{a_i-t}^{a_i} \beta(b) db], & a_i > t; \\ i(0, t - a_i) exp[-\int_0^{a_i} \beta(b) db], & a_i \leq t. \end{cases} \tag{24}$$

From (5), (7), and (24) with $\nu = 0$, for $t \geq 0$,

$$S'(t) = -i(0,t) \implies S(0) - S_\infty = \int_0^\infty i(0,t) dt. \tag{25}$$

Preprints (www.preprints.org) | NOT PEER-REVIEWED | Posted: 27 November 2023 doi:10.20944/preprints202311.1686.v1

For $t \geq 0$, (24) and (25) imply

$$\begin{aligned}
&\int_0^\infty \int_r^{r+s} \alpha(a_i) i(a_i,t) da_i dt \\
&= \int_r^{r+s} \alpha(a_i) \left(\int_0^{a_i} i(a_i,t) dt + \int_{a_i}^\infty i(a_i,t) dt \right) da_i \\
&= \int_r^{r+s} \alpha(a_i) \left(\int_0^{a_i} i_0(a_i - t) e^{-\int_{a_i - t}^{a_i} \beta(b) db} dt + \int_{a_i}^\infty i(0, t - a_i) e^{-\int_0^{a_i} \beta(b) db} dt \right) da_i \\
&= \int_r^{r+s} \alpha(a_i) \left(-\int_{a_i}^0 i_0(u) e^{-\int_u^{a_i} \beta(b) db} du + \int_0^\infty i(0,u) e^{-\int_0^{a_i} \beta(b) db} du \right) da_i \\
&= \int_r^{r+s} \alpha(a_i) \left(\int_0^{a_i} i_0(u) e^{-\int_u^{a_i} \beta(b) db} du + \left(\int_0^\infty i(0,u) du \right) \left(e^{-\int_0^{a_i} \beta(b) db} \right) \right) da_i \\
&= \Gamma + (S(0) - S_\infty)\Lambda.
\end{aligned}$$

Then, (12) follows from (15). □

Remark. We claim that $|E'(t) + I'(t)|$ is bounded for $t \geq 0$. We shall prove this statement in two cases. For $t \geq r + s$, (7), (22), and (24) imply there exists $C_1 > 0$ such that

$$\begin{aligned}
i(r+s,t) &= i(0, t-r-s) exp\left[-\int_0^{r+s} \beta(b) db \right] \\
&\leq \left(\int_r^{r+s} \alpha(a_i) i(a_i, t-r-s) da_i \right) \\
&\quad \left(S(t-r-s) + \int_0^{t-r-s} \sigma(a_i) v(a_v, t-r-s) da_v \right) \\
&\leq \left(\bar{\alpha} I(t-r-s) \right) \left(S(t-r-s) + \bar{\sigma} V(t-r-s) \right) \leq C_1.
\end{aligned}$$

For $t < r + s$, we again use (24) to derive

$$i(r+s,t) = i_0(r+s-t) exp\left[-\int_{r+s-t}^{r+s} \beta(b) db \right] \leq i_0(r+s-t).$$

Since the initial condition i_0 is piecewise continuous on $[0, r+s)$, there exists $C_2 > 0$ such that

$$i(r+s,t) \leq i_0(r+s-t) \leq C_2,$$

for $t < r + s$.

Let $C^* = \max\{C_1, C_2\}$. Combining (7), (18), and (19), we have, for $t \geq 0$,

$$\begin{aligned}
\left| E'(t) + I'(t) \right| &= \left| i(0,t) - i(r+s,t) - \int_0^{r+s} \beta(a_i) i(a_i,t) da_i \right| \\
&= \left| \left(\int_r^{r+s} \alpha(a_i) i(a_i,t) da_i \right) \left(S(t) + \int_0^t \sigma(a_v) v(a_v,t) da_v \right) \right. \\
&\quad \left. - i(r+s,t) - \int_0^{r+s} \beta(a_i) i(a_i,t) da_i \right| \\
&\leq \bar{\alpha} I(t) \left(S(t) + \bar{\sigma} V(t) \right) + C^* + \bar{\beta} \left(E(t) + I(t) \right).
\end{aligned}$$

By (22), $|E'(t) + I'(t)|$ is bounded for $t \geq 0$.

Preprints (www.preprints.org) | NOT PEER-REVIEWED | Posted: 27 November 2023 doi:10.20944/preprints202311.1686.v1

2.3. Application of the Model to the 2003 SARS Epidemic in Taiwan

This example is based on results in [4–7], and illustrates the case that the period of infectiousness coincides with the symptomatic period. In the SARS epidemic in Taiwan in 2003, the seriousness of the disease was recognized after an initial period, and by April 24, 2003, infected individuals were quickly identified and isolated in hospitals, with stringent control measures to prevent further disease transmission. The incubation period of SARS was from two to seven days. In this epidemic in Taiwan 2003, vaccination was not available. We first consider the model without vaccination ($\nu = 0$).

We assume that the incubation (exposed) period lasts from the moment of infection to day 5, and the infectious period lasts from day 5 to day 26. We overlap the symptomatic and infectious periods, and assume that after April 24, 2003, a certain percentage of symptomatic infectives were isolated in hospitals, and gave no further transmissions to susceptibles. We will then extrapolate the model to the case that the period of symptoms and infectiousness overlapped one day and the case that the period of symptoms and infectiousness overlapped two days (see Figure 2).

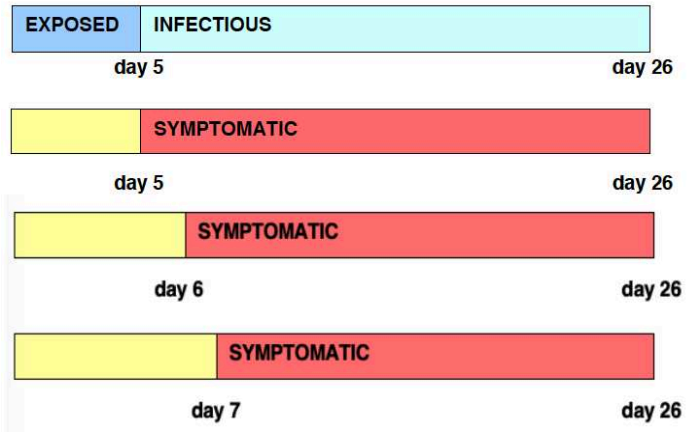

Figure 2. Timeline of infectious periods relative to symptom onset for SARS. The top segment displays the exposed-infectious period. Segments 2 to 4 illustrate scenarios where the infectious period coincides with the symptomatic period, precedes the symptomatic period by one day, and precedes the symptomatic period by two days, respectively.

All parameters are based on fitting the model to data ([4]). The initial population of susceptibles is set at $S(0) = 6.0 \times 10^6$. It is assumed that the exposed period lasts from day 0 until day $r = 5$, and the infectious period lasts $s = 21$ days, from day $r = 5$ to day $r + s = 26$. The asymptomatic period and the exposed period coincide, as do the symptomatic period and the infectious period (see Figure 2). The transmission rate is defined as (see Figure 3):

$$\alpha(a_i) = \begin{cases} 0 & \text{if } 0 \le a_i < r, \\ 3.1 \times 10^{-8}(a_i - r) & \text{if } r \le a_i < r + 10, \\ 3.1 \times 10^{-7}\left(1.0 - \frac{a_i - r - 10}{11}\right) & \text{if } r + 10 \le a_i < r + s, \\ 0 & \text{if } r + s \le a_i. \end{cases}$$

The hospitalization rate is 54.5% per day after manifestation of symptoms at day 5 and 0.0% per day before day 5 (see Figure 3):

$$\beta_H(a_i) = \begin{cases} 0 & \text{if } 0 \le a_i < 5, \\ .545 & \text{if } 5 \le a_i \le 26. \end{cases}$$

Preprints (www.preprints.org) | NOT PEER-REVIEWED | Posted: 27 November 2023 doi:10.20944/preprints202311.1686.v1

We assume only pre-symptomatic infected individuals are quarantined. The quarantine rate is 2.0% per day from day 0 to day 5 and then 0.0% per day after day 5 (see Figure 3):

$$\beta_Q(a_i) = \begin{cases} .020 & \text{if } 0 \le a_i < 5, \\ 0 & \text{if } 5 \le a_i \le 26. \end{cases}$$

It is assumed that at time 0 the distribution of infectives $i(a_i, 0)$ is given by (see Figure 3):

$$i(a_i,0) = \begin{cases} 12 & \text{if } a_i \le 1, \\ 5 & \text{if } 1 < a_i \le 2, \\ 19 & \text{if } 2 < a_i \le 3, \\ 9 & \text{if } 3 < a_i \le 4, \\ 15 & \text{if } 4 < a_i \le 5, \\ \frac{1}{2}(17-a) & \text{if } 5 < a_i \le 17, \\ 0 & \text{if } 17 < a_i. \end{cases}$$

With this initial distribution $i(a, 0)$, the total number of exposed at time $t = 0$ is $E(0) = 60$ and the total number of infectious at time $t = 0$ is $I(0) = 36$. It is assumed that $H(0) = 0$, $Q(0) = 0$, and $R(0) = 0$. In Figure 4 the graphs of the exposed population $E(t)$, the infectious population $I(t)$, the cumulative number of new cases $\int_0^t i(0, \hat{t})d\hat{t}$, and the daily number of new cases $i(0, t)$ are given and compared to the data of the epidemic from April 28 to June 25, 2003. The total number of new cases is ≈ 230. Data for the epidemic is given in [4], with 232 cases reported for this time period.

The model can be used to evaluate the role of the susceptible size population $S(0)$ in predicting the number of cases $S(0) - S_\infty$ in the epidemic, with all other parameters and initial conditions held fixed. For this example, $S(0) = 6,000,000$ and $S_0 - S_\infty \approx 230$. In Figure 5, we use the formula (12) to plot $S(0) - S_\infty$ as a function of $S(0)$, as $S(0)$ increases from 10^5 to 10^7. We find that the number of cases $S(0) - S_\infty$ increases as the initial susceptible population size $S(0)$ increases.

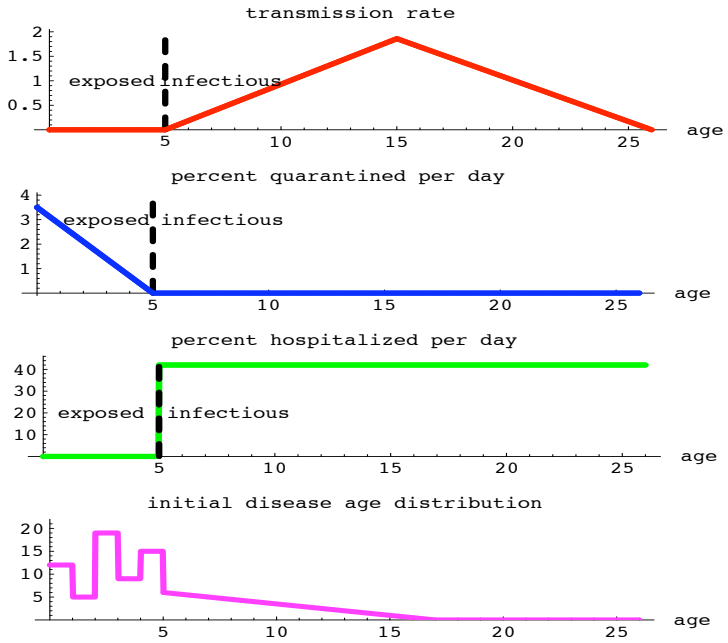

Figure 3. The disease age-dependent transmission rate, quarantine rate, hospitalization rate, and initial disease age distribution of infectives for the 2003 Taiwan SARS epidemic from April 28 to June 5, 2003.

Preprints (www.preprints.org) | NOT PEER-REVIEWED | Posted: 27 November 2023 doi:10.20944/preprints202311.1686.v1

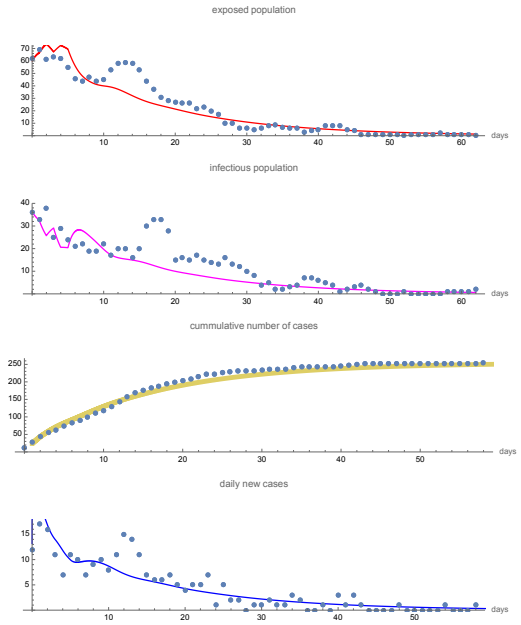

Figure 4. The graphs of the exposed class $E(t)$, infectious class $I(t)$, cumulative number of new cases, and daily new cases in the 2003 Taiwan SARS epidemic from April 28 to June 5. The dotted curves are data (Taiwan Centers for Disease Control https://www.cdc.gov.tw) and the solid curves are the model simulation. $S_\infty \approx 5,999,770$. The cumulative number of cases on June 5 is approximately 230.

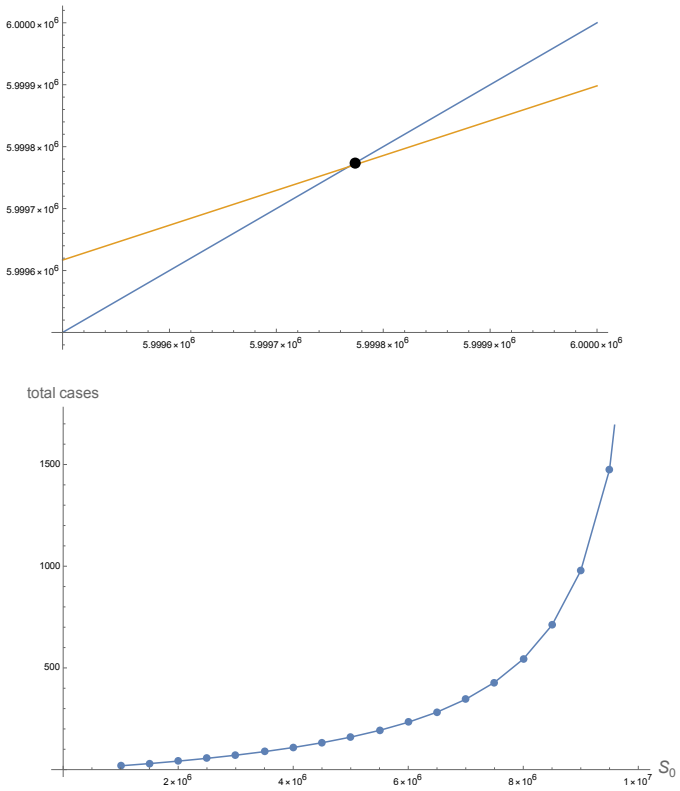

Figure 5. (Top) The blue graph is the function $F(X) = X$ and the red graph is the function $G(X) = exp[-(\Gamma + (S(0) - X)\Lambda)]S(0)$. The intersection of the two graphs is (S_∞, S_∞), $S_\infty \approx 5,999,770$. $\Lambda \approx 9.376 \times 10^{-8}$ and $\Gamma \approx 0.000016929$. The total number of cases is $S(0) - S_\infty \approx 230$. (Bottom) The number of new cases $S(0) - S_\infty$ as a function of $S(0)$, where S_∞ is computed by $S_\infty = exp[-(\Gamma + (S(0) - S_\infty)\Lambda)]S(0)$. $S(0) - S_\infty$ increases as $S(0)$ increases.

Preprints (www.preprints.org) | NOT PEER-REVIEWED | Posted: 27 November 2023 doi:10.20944/preprints202311.1686.v1

Remark. The asymptotic behavior of the solutions of (5), (6), (7) without vaccination ($\nu = 0$), is analogous to the asymptotic behavior of the solutions of the classic Kermack-McKendrick SEIR model [8,9]:

$$S'(t) = -\alpha S(t)I(t), t \geq 0, \tag{26}$$

$$E'(t) = \alpha S(t)I(t) - \beta E(t), t \geq 0, \tag{27}$$

$$I'(t) = \beta E(t) - \gamma I(t), t \geq 0, \tag{28}$$

$$R'(t) = \gamma I(t), t \geq 0. \tag{29}$$

The limiting behavior as $t \to \infty$ depends on the initial conditions $S(0), E(0), I(0)$:

$$\lim_{t\to\infty} E(t) = 0, \lim_{t\to\infty} I(t) = 0, \lim_{t\to\infty} S(t) = S_\infty > 0,$$

where S_∞ satisfies

$$S_\infty = S(0) + E(0) + I(0) + \frac{\gamma}{\alpha} log\left(\frac{S_\infty}{S(0)}\right). \tag{30}$$

Examples are given in Figure 6. This result is of major scientific importance because it explains why epidemic diseases, which can occur hundreds of thousands of times over evolutionary time scales, do not annihilate biological species.

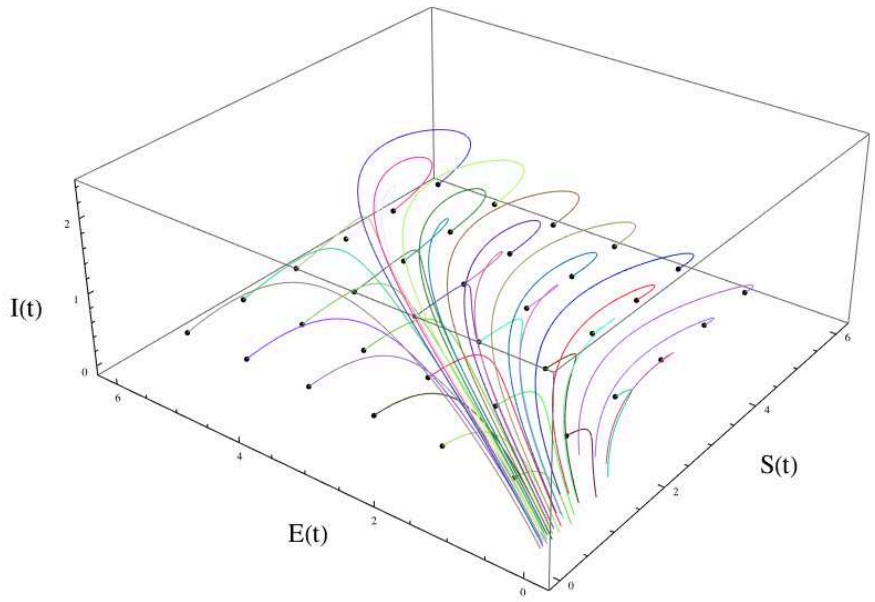

Figure 6. The solution $S(t), E(t), I(t)$ of the Kermack-McKendrick SEIR model (26), (27), (28), (29) for varying initial values $S(0), E(0), I(0)$. The limiting behavior as $t \to \infty$ is dependent on the initial values: $\lim_{t\to\infty} E(t) = 0$, $\lim_{t\to\infty} I(t) = 0$, $\lim_{t\to\infty} S(t) = S_\infty$, where S_∞ satisfies (30).

The role of hospitalization (isolation) and quarantine of infectives in the 2003 Taiwan SARS epidemic can be analyzed in the model. We consider two scenarios in which the infection period precedes the symptomatic period - the period of infectiousness begins on day 5 and the period of symptoms begins on day 6 or day 7 (see Figure 2). We also consider three scenarios in which the

Preprints (www.preprints.org) | NOT PEER-REVIEWED | Posted: 27 November 2023 doi:10.20944/preprints202311.1686.v1

quarantine rate is 2.0 % per day, 4.0% per day, and 10.0% per day. We assume only pre-symptomatic infected individuals are quarantined. The parameters α and β_H are as before, and $\nu = 0$ (no vaccination).

In the case that exposed infectives are symptomatic at day 6 (infectious 1 day before symptoms) and the maximum quarantine rate is 2.0%, the cumulative number of cases reaches 2000 in 1 year and the cumulative number of quarantined reaches 150 in 1 year. In the case that exposed infectives are symptomatic at day 7 (infectious 2 days before symptoms) and the maximum quarantine rate is 2.0%, the cumulative number of cases is approximately 3,700,000 and the cumulative number of quarantined reaches 300,000 in 1 year. (see Figure 7)

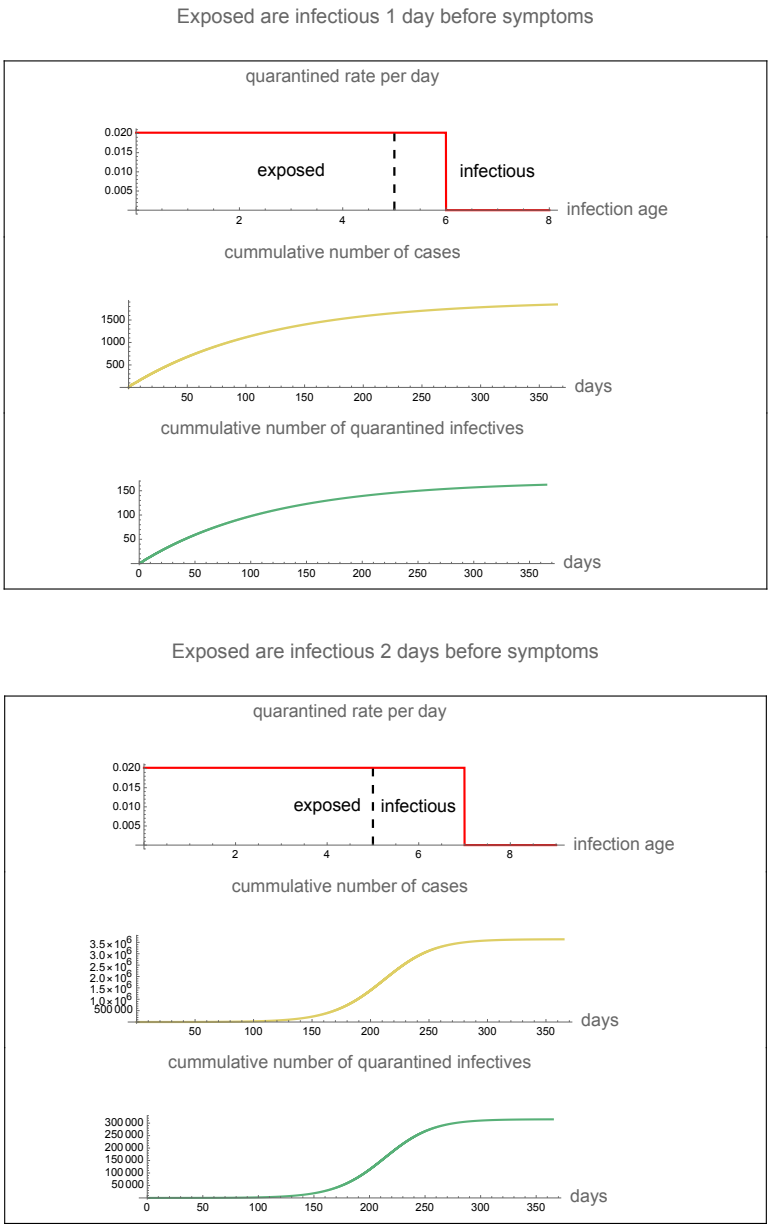

Figure 7. The epidemic in the case that infectiousness precedes symptom on-set by 1 day and the maximum quarantine rate is 2.0% (top) and infectiousness precedes symptom on-set by 2 days and the maximum quarantine rate is 2.0% (bottom). Vertical dashed lines separate exposed and infectious. Red vertical lines represent the beginning of symptoms and the maximum disease age of quarantine.

Preprints (www.preprints.org) | NOT PEER-REVIEWED | Posted: 27 November 2023 doi:10.20944/preprints202311.1686.v1

In the case that exposed infectives are symptomatic at day 6 (infectious 1 day before symptoms) and the maximum quarantine rate is 4.0%, the cumulative number of cases reaches approximately 800 in 150 days and the cumulative number of quarantined reaches 120 in 150 days. In the case that exposed infectives are symptomatic at day 7 (infectious 2 days before symptoms) and the maximum quarantine rate is 4.0%, the cumulative number of cases is approximately 2,700,000 in 450 days and the cumulative number of quarantined reaches 400,000 in 450 days. (see Figure 8)

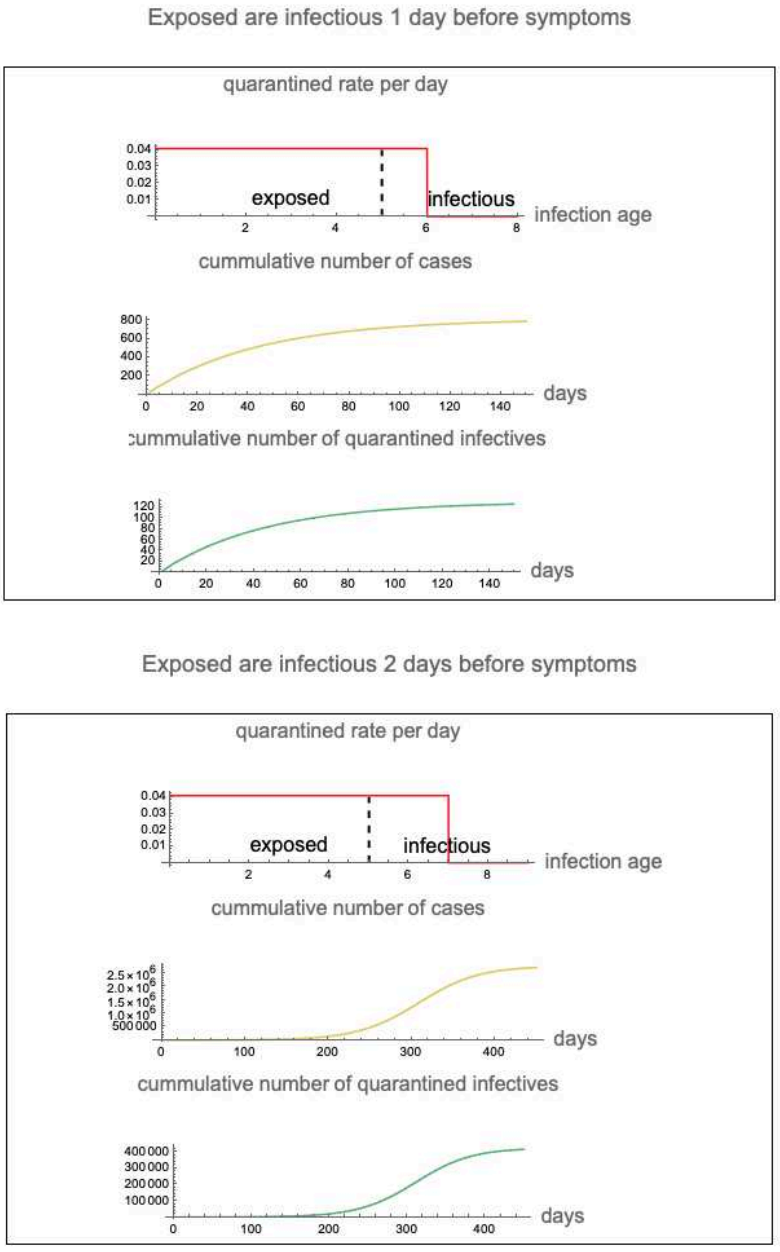

Figure 8. The epidemic in the case that infectiousness precedes symptom on-set by 1 day and the maximum quarantine rate is 4.0% (top) and infectiousness precedes symptom on-set by 2 days and the maximum quarantine rate is 4.0% (bottom). Vertical dashed lines separate exposed and infectious. Red vertical lines represent the beginning of symptoms and the maximum disease age of quarantine.

In the case that exposed infectives are symptomatic at day 6 (infectious 1 day before symptoms) and the maximum quarantine rate is 10.0%, the cumulative number of cases reaches approximately

Preprints (www.preprints.org) | NOT PEER-REVIEWED | Posted: 27 November 2023 doi:10.20944/preprints202311.1686.v1

350 in 50 days and the cumulative number of quarantined is approximately 100 in 50 days. In the case that exposed infectives are symptomatic at day 7 (infectious 2 days before symptoms) and the maximum quarantine rate is 10.0%, the cumulative number of cases is approximately 1,000 in 200 days and the cumulative number of quarantined reaches approximately 300 in 200 days. (see Figure 9)

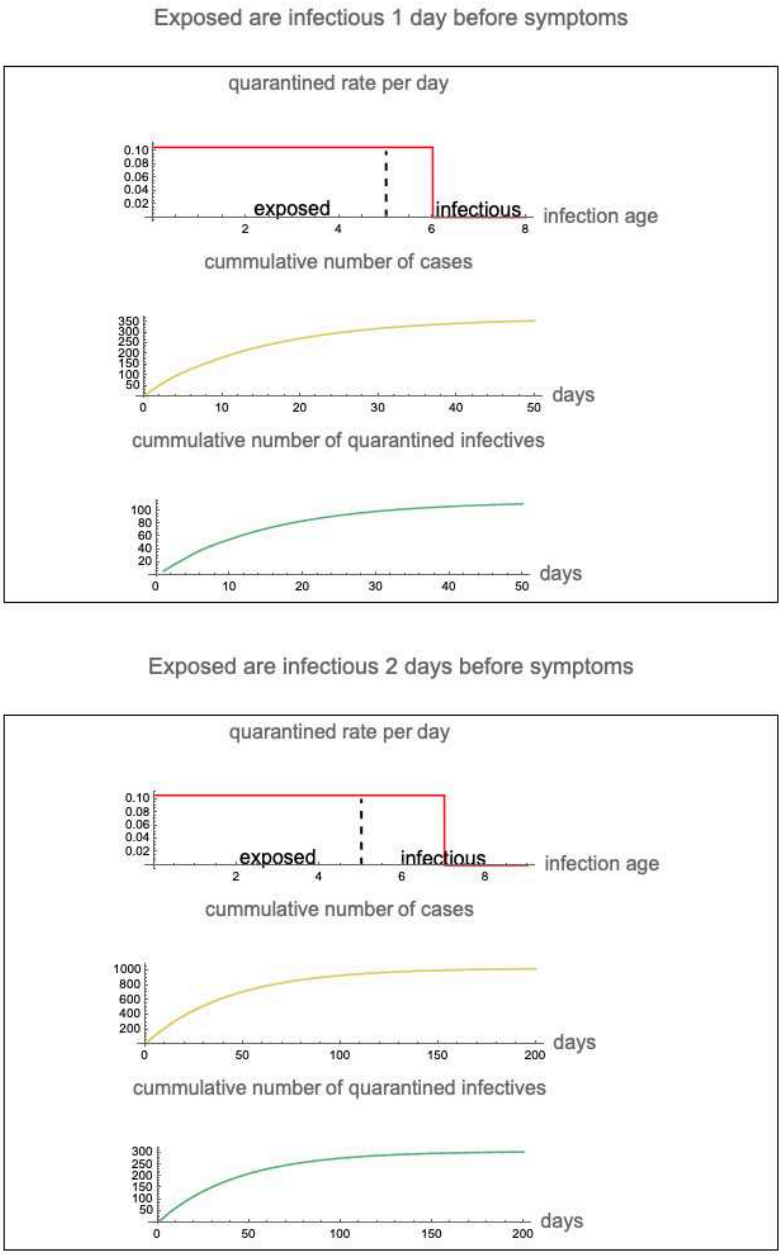

Figure 9. The epidemic in the case that infectiousness precedes symptom on-set by 1 day and the maximum quarantine rate is 10.0% (top) and infectiousness precedes symptom on-set by 2 days and the maximum quarantine rate is 10.0% (bottom). Vertical dashed lines separate exposed and infectious. Red vertical lines represent the beginning of symptoms and the maximum disease age of quarantine.

For the disease age structured model (5), (6), (7), without vaccination ($\nu = 0$), the epidemic reproduction number ([7]) R_0 of the epidemic is

$$R_0 = S(0) \int_r^{r+s} \alpha(a_i) exp\left(- \int_0^{a_i} \Big(\beta_Q(b) + \beta_H(b)\Big) db \right) da_i.$$

Preprints (www.preprints.org) | NOT PEER-REVIEWED | Posted: 27 November 2023 doi:10.20944/preprints202311.1686.v1

The reproduction number R_0 is the number of secondary infections generated by 1 infected individual over the disease course. For the parameters s, r, $I_0(a_i)$, $\alpha(a_i)$ and $\beta_H(a_i)$ as before, R_0 is graphed as a function of the number of days infectiousness pre-symptomatic p and the maximum quarantined rate in Figure 10. If $R_0 > 1$, then the epidemic is severe, although it ultimately subsides as the susceptible population is exhausted. In Figure 11 the graph of the total number of cases $\int_0^\infty i(0,t)dt$ as a function of the number of days of infectiousness pre-symptomatic p and the maximum quarantine rate is given. The number of cases rises sharply as the quarantine rate falls below 5% and the number of days infectious pre-symptomatic exceeds 1.

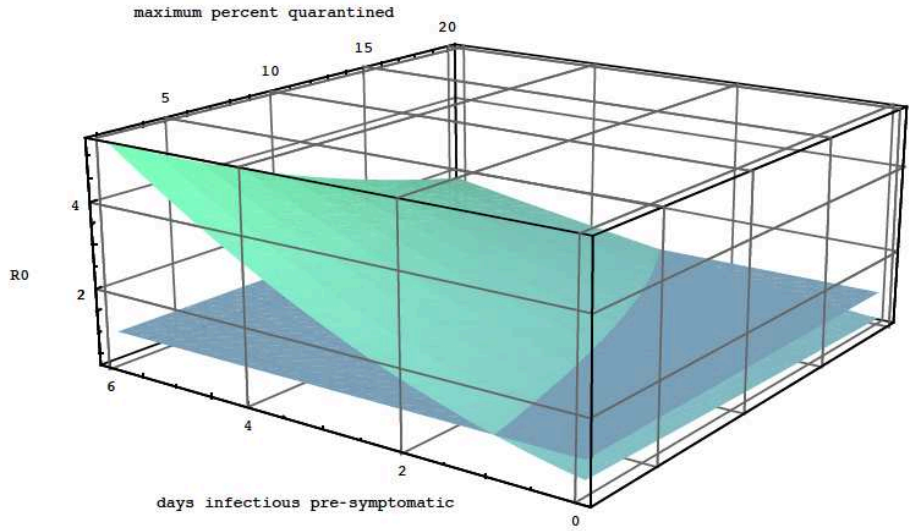

Figure 10. The epidemic reproductive number R_0 graphed as a function of the number of days infectiousness pre-symptomatic and the maximum quarantine rate.

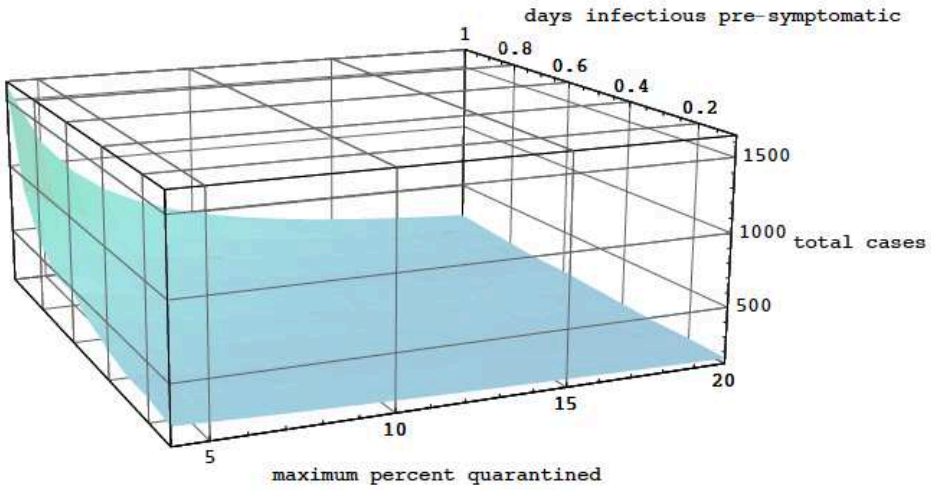

Figure 11. The total number of cases graphed as a function of the number of days infectiousness pre-symptomatic and the maximum quarantine rate.

Preprints (www.preprints.org) | NOT PEER-REVIEWED | Posted: 27 November 2023 doi:10.20944/preprints202311.1686.v1

We modify the model of the 2003 Taiwan SARS epidemic without vaccination to include vaccination, which was not available in Taiwan in 2003. This example will illustrate the epidemic evolution with alternate elements, including vaccination. We take the vaccination parameter $\nu = 0.05$. Vaccinated individuals begin with vaccinated age $a_v = 0$ and then acquire increasing immunity as their vaccination age increases over a period of days or weeks. The total number of vaccinated at time t is $\int_0^t v(a_v, t)da_v$. Susceptibles are vaccinated at a constant rate ν per day. The proportion of vaccinated still susceptible at vaccination age a_v is $\sigma(a_v)$.

In this example $\nu = 0.05$, $\sigma(a_v) = .7e^{-.25a_v} + .3$ (which means vaccination results in incomplete immunity, and as vaccination age a_v advances, 30% of vaccinated individuals remain susceptible). We assume, $V(0) = 0$. Infectiousness precedes symptom onset by 2 days and the maximum quarantine rate is 4.0%. All other parameters are as before. The evolution of the epidemic is graphed in Figure 12, where it is seen that the cumulative number of cases is approximately 175,000. This example can be compared to the model with the same parameters, except without vaccination in the bottom graph in Figure 8, where the cumulative number of cases is approximately 350,000.

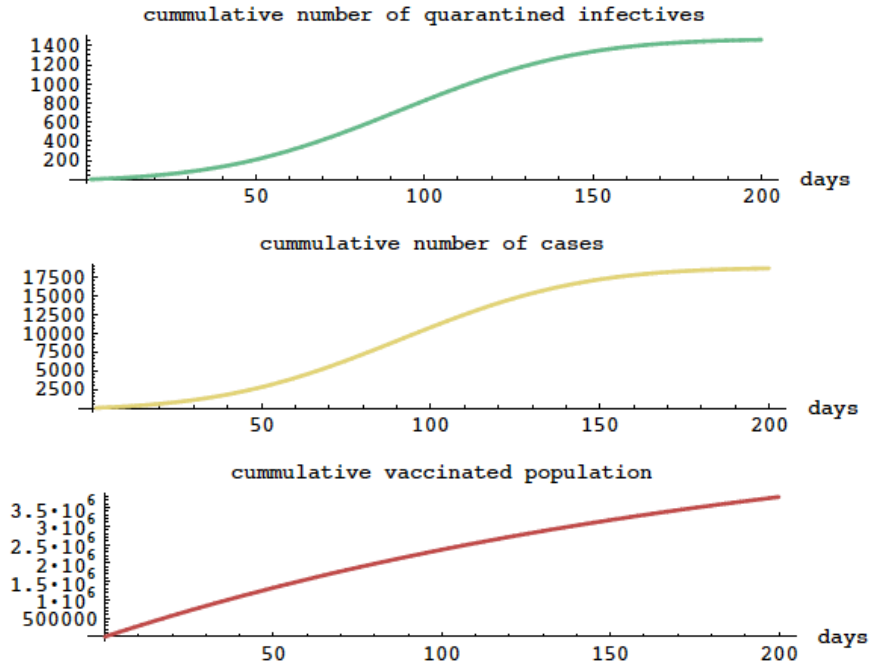

Figure 12. The cumulative number of quarantined cases, total number of cases, and cumulative number of vaccinated susceptibles in the model with vaccination.

2.4. Application of the Model to the COVID-19 Epidemic in New York State

In this section, we apply our mathematical model to analyze the transmission dynamics of COVID-19 in New York State. Numerous factors influence COVID-19 transmission, including vaccination rates, the emergence of more contagious variants, the public's reaction to and understanding of the virus, and governmental responses and policies. To provide a more detailed analysis, we segment the data into different phases, aligned with the timeline of COVID-19 transmission and the New York State government's response [9].

Preprints (www.preprints.org) | NOT PEER-REVIEWED | Posted: 27 November 2023 doi:10.20944/preprints202311.1686.v1

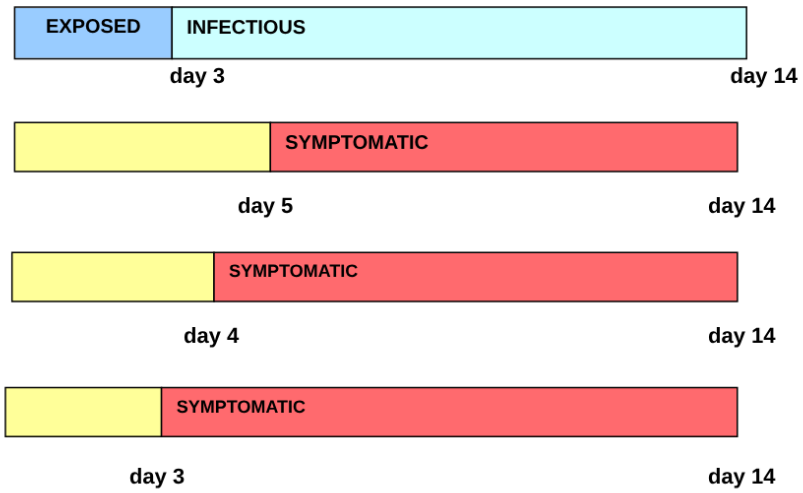

Figure 13. Timeline of infectious periods relative to symptom onset for COVID-19. The top segment displays the exposed-infectious period. Segments 2 to 4 illustrate scenarios where the infectious period starts two days before, one day before, and simultaneously with symptom onset, respectively.

We obtain data from the New York State Department of Health (https://health.data.ny.gov/). The state of New York confirmed its first case of COVID-19 during the pandemic on March 1, 2020, while the first complete vaccination (i.e., two-dose vaccination) began on December 15, 2020. Our analysis focuses on the timeframe from October 30, 2020, to March 13, 2022.

In Figure 14, the green dots depict daily reported cases. Since this data tends to be erratic and is subject to ongoing updates, a standard approach is to use a rolling weekly average. Accordingly, the gray bars in the figure represent this rolling weekly average. The top figure in Figure 15 follows a similar presentation: green dots for daily vaccinated individuals and gray bars for the rolling weekly averages.

On average, symptoms of COVID-19 manifest in newly infected individuals approximately 5-6 days later (*WebMD*, https://www.webmd.com/covid/coronavirus-incubation-period) and last for about two weeks. We set the minimum age of infectiousness $r = 3$, the number of days of pre-symptomatic infectiousness $p = 2$, the number of days when symptoms appear $r + p = 5$, and the number of days of infectiousness $s = 11$. It is assumed that the hospitalization rate $\beta_H(a_i)$ per day is 54.5% once symptoms appear (after day $r + p = 5$), with a rate of 0.0% per day before day 5 (Figure 16).

$$\beta_H(a_i) = \begin{cases} 0 & \text{if } 0 \le a_i < r + p, \\ .545 & \text{if } r + p \le a_i \le 14. \end{cases}$$

We assume only pre-symptomatic infected individuals are quarantined. The quarantine rate is 4.0% per day from day 0 to day 5 and then 0.0% per day after day 5 (see Figure 16)

$$\beta_Q(a_i) = \begin{cases} .020 & \text{if } 0 \le a_i < r + p, \\ 0 & \text{if } r + p \le a_i \le 14. \end{cases}$$

Preprints (www.preprints.org) | NOT PEER-REVIEWED | Posted: 27 November 2023 doi:10.20944/preprints202311.1686.v1

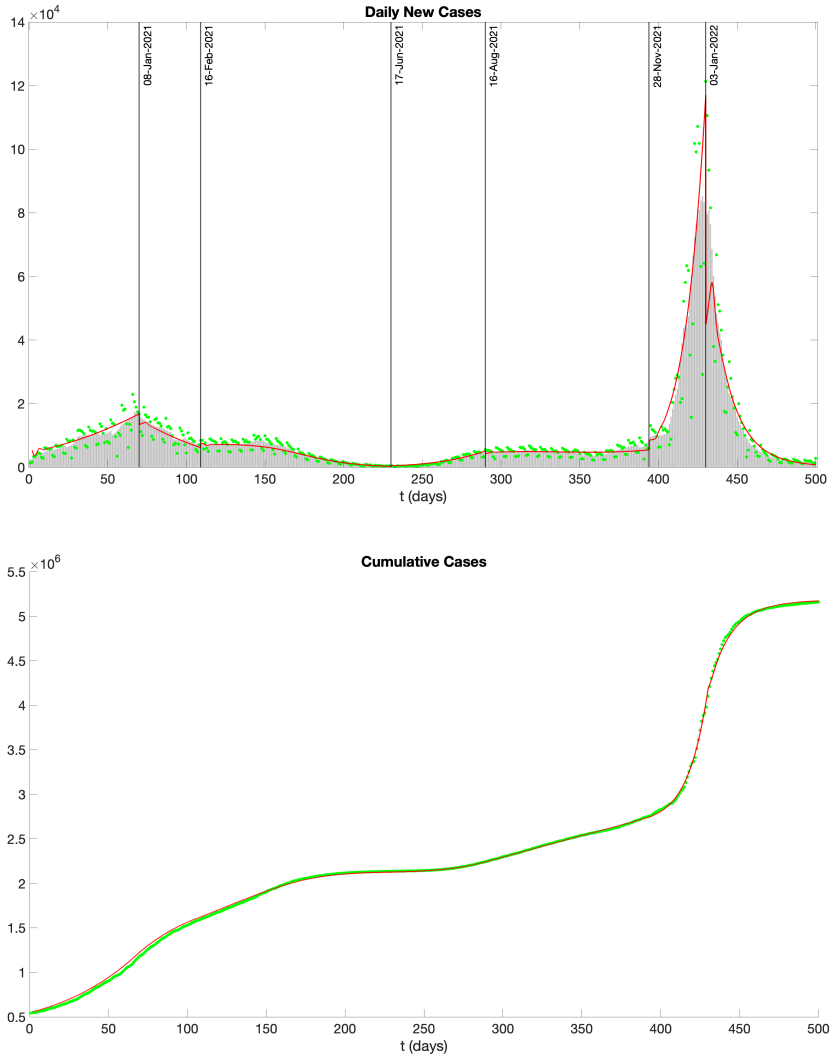

Figure 14. Daily and cumulative infectious cases for COVID-19 in New York State from October 30, 2020, to March 13, 2022. (Top) Green dots represent data sourced from the New York State Department of Health (https://health.data.ny.gov/Health/New-York-State-Statewide-COVID-19-Testing/jvfi-ffup), gray bars show the rolling weekly averages, and the red curve is the simulation result of our model. (Bottom) Green dots represent data, and the red curve is the simulation result of our model.

Preprints (www.preprints.org) | NOT PEER-REVIEWED | Posted: 27 November 2023 doi:10.20944/preprints202311.1686.v1

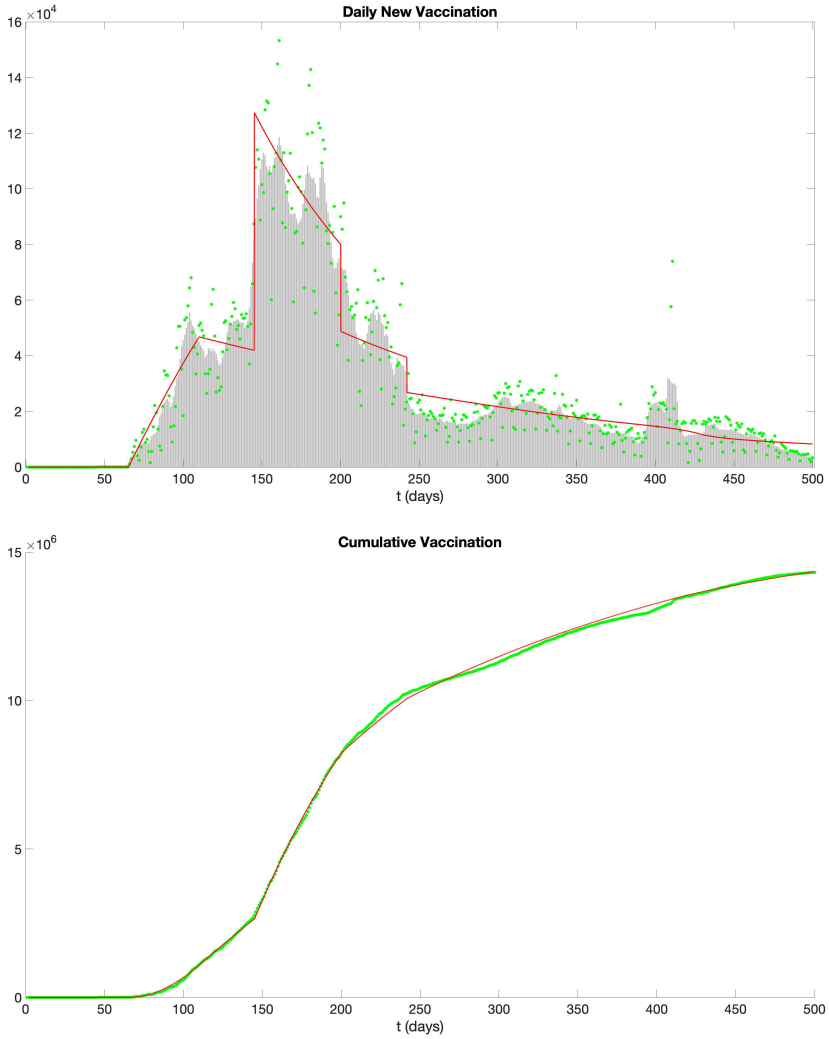

Figure 15. Daily and cumulative COVID-19 vaccinations in New York State from October 30, 2020, to March 13, 2022. (Top) Green dots represent data from the New York State Department of Health (https://health.data.ny.gov/Health/New-York-State-Statewide-COVID-19-Vaccination-Data/duk7-xrni), gray bars represent the rolling weekly average, and the red curve is the simulation result of our model. (Bottom) The green dotted curve is data, and the red curve illustrates the outcomes from our model simulation.

In the case of COVID-19, the infectious period precedes the symptomatic phase. Individuals with COVID-19 can transmit the virus up to 48 hours before they begin to show symptoms. Based on this understanding, we assume the exposed period for COVID-19 spans from the moment of infection to day 3 (i.e., $r = 3$). The infectious period then continues from day 3 to day 14, resulting in a two-day overlap between the onset of symptoms and infectiousness (see Figure 13). As mentioned, many factors influence the transmission of COVID-19. Therefore, we divide the entire timeframe into different phases. Upon fitting the data, we have different values of transmission rate in different phases:

Preprints (www.preprints.org) | NOT PEER-REVIEWED | Posted: 27 November 2023 doi:10.20944/preprints202311.1686.v1

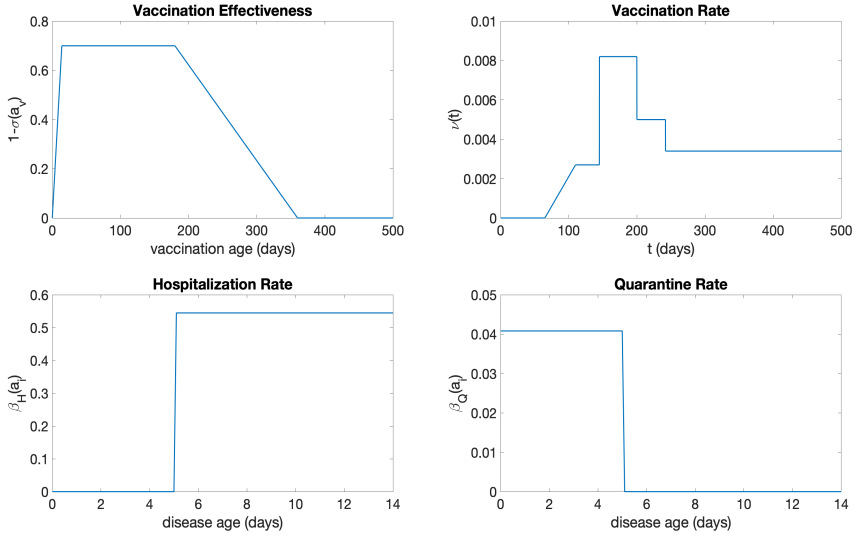

Figure 16. The vaccination age-dependent effectiveness, vaccination rate, hospitalization rate, and quarantine rate for the COVID-19 epidemic in New York State from October 30, 2020, to March 13, 2022.

- Phase 1 (11/01/2020 – 01/08/2021) There was no vaccination in this phase.

$$\alpha(a_i) = \begin{cases} 0 & \text{if } 0 \le a_i < r, \\ 8.4 \times 10^{-9}(a_i - r) & \text{if } r \le a_i < r+7, \\ 8.4 \times 10^{-9} \times \frac{7}{s-7}(r+s-a_i) & \text{if } r+7 \le a_i < r+s, \\ 0 & \text{if } r+s \le a_i. \end{cases}$$

- Phase 2 (01/08/2021 – 02/16/2021) With the commencement of vaccination campaigns and growing public caution, there was a small decrease in the COVID-19 transmission rate.

$$\alpha(a_i) = \begin{cases} 0 & \text{if } 0 \le a_i < r, \\ 6.7 \times 10^{-9}(a_i - r) & \text{if } r \le a_i < r+7, \\ 6.7 \times 10^{-9} \times \frac{7}{s-7}(r+s-a_i) & \text{if } r+7 \le a_i < r+s, \\ 0 & \text{if } r+s \le a_i. \end{cases}$$

- Phase 3 (02/16/2021 – 06/17/2021) The emergence and prevalence of the Alpha variant [10] brought a small increase in the transmission rate.

$$\alpha(a_i) = \begin{cases} 0 & \text{if } 0 \le a_i < r, \\ 8.3 \times 10^{-9}(a_i - r) & \text{if } r \le a_i < r+7, \\ 8.3 \times 10^{-9} \times \frac{7}{s-7}(r+s-a_i) & \text{if } r+7 \le a_i < r+s, \\ 0 & \text{if } r+s \le a_i. \end{cases}$$

Preprints (www.preprints.org) | NOT PEER-REVIEWED | Posted: 27 November 2023 doi:10.20944/preprints202311.1686.v1

- Phase 4 (06/17/2021 – 08/16/2021) In June 2021, the arrival of the Delta variant [11] led to a rapid surge in COVID-19 cases. It is estimated that the Delta variant is 60%–90% more transmissible than the Alpha variant [11,12].

$$\alpha(a_i) = \begin{cases} 0 & \text{if } 0 \le a_i < r, \\ 17.7 \times 10^{-9}(a_i - r) & \text{if } r \le a_i < r+7, \\ 17.7 \times 10^{-9} \times \frac{7}{s-7}(r+s-a_i) & \text{if } r+7 \le a_i < r+s, \\ 0 & \text{if } r+s \le a_i. \end{cases}$$

- Phase 5 (08/16/2021 – 11/28/2021) In response to the rise of the Delta variant in August 2021, policies such as a universal mask mandate for all public and private schools were implemented [9], leading to a reduced transmission rate.

$$\alpha(a_i) = \begin{cases} 0 & \text{if } 0 \le a_i < r, \\ 14.2 \times 10^{-9}(a_i - r) & \text{if } r \le a_i < r+7, \\ 14.2 \times 10^{-9} \times \frac{7}{s-7}(r+s-a_i) & \text{if } r+7 \le a_i < r+s, \\ 0 & \text{if } r+s \le a_i. \end{cases}$$

- Phase 6 (11/28/2021 – 01/03/2022) The Omicron variant [13] was first discovered in Botswana and South Africa in November 2021 and quickly spread to other countries, including the United States. In December 2021, the emergence of the Omicron variant led to a significant surge in COVID-19 cases.

$$\alpha(a_i) = \begin{cases} 0 & \text{if } 0 \le a_i < r, \\ 23.6 \times 10^{-9}(a_i - r) & \text{if } r \le a_i < r+7, \\ 23.6 \times 10^{-9} \times \frac{7}{s-7}(r+s-a_i) & \text{if } r+7 \le a_i < r+s, \\ 0 & \text{if } r+s \le a_i. \end{cases}$$

- Phase 7 (01/03/2022 – 03/13/2022) Reacting to the emergence of the Omicron variant, various preventive policies, such as mask mandates and "Comprehensive Winter Surge Plans", were introduced [9], leading to a decrease in the transmission rate.

$$\alpha(a_i) = \begin{cases} 0 & \text{if } 0 \le a_i < r, \\ 8.7 \times 10^{-9}(a_i - r) & \text{if } r \le a_i < r+7, \\ 8.7 \times 10^{-9} \times \frac{7}{s-7}(r+s-a_i) & \text{if } r+7 \le a_i < r+s, \\ 0 & \text{if } r+s \le a_i. \end{cases}$$

The transmission rate $\alpha(a_i, t)$ as a function of disease age a_i and time t is depicted in Figure 17.

Preprints (www.preprints.org) | NOT PEER-REVIEWED | Posted: 27 November 2023 doi:10.20944/preprints202311.1686.v1

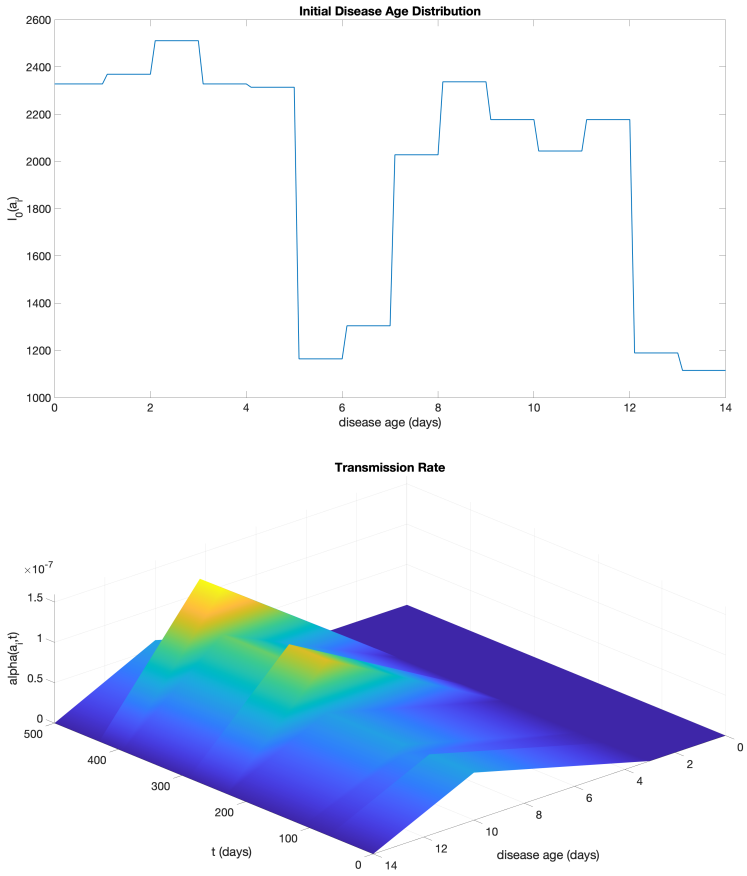

Figure 17. (Top) The initial disease age distribution and (bottom) the phase-dependent disease transmission rate, as a function of the disease age a_i and time t, for the COVID-19 epidemic in New York State from October 30, 2020, to March 13, 2022.

Similar to the example of SARS, we utilize the daily reported data from October 16, 2020, to October 29, 2020 (a 14-day period before October 30, 2020) as the initial distribution of $i(a_i, 0)$. Specific, at $t = 0$,

$$i(a_i,0) = \begin{cases} 2328 & \text{if } a_i \le 1, \\ 2369 & \text{if } 1 < a_i \le 2, \\ 2511 & \text{if } 2 < a_i \le 3, \\ 2328 & \text{if } 3 < a_i \le 4, \\ 2314 & \text{if } 4 < a_i \le 5, \\ 1164 & \text{if } 5 < a_i \le 6, \\ 1304 & \text{if } 6 < a_i \le 7, \\ 2028 & \text{if } 7 < a_i \le 8, \\ 2337 & \text{if } 8 < a_i \le 9, \\ 2177 & \text{if } 9 < a_i \le 10, \\ 2044 & \text{if } 10 < a_i \le 11, \\ 2177 & \text{if } 11 < a_i \le 12, \\ 1189 & \text{if } 12 < a_i \le 13, \\ 1115 & \text{if } 13 < a_i \le 14. \end{cases}$$

Preprints (www.preprints.org) | NOT PEER-REVIEWED | Posted: 27 November 2023 doi:10.20944/preprints202311.1686.v1

The graph of this initial disease age distribution $i(a_i, 0)$ is plotted in Figure 16. We assume $S(0) = 19,500,000$ (https://usafacts.org/data/topics/people-society/population-and-demographics/).

In contrast to the SARS outbreak in Taiwan in 2003, where vaccination was not an option, the availability and administration of COVID-19 vaccines have significantly influenced the dynamics of its transmission. While COVID-19 vaccines have proven to offer substantial protection to those who are susceptible, they are not infallible—people can still get COVID-19 after vaccination. This means that the COVID-19 vaccination is not 100% effective. We assume that the vaccination age-dependent function $\sigma(a_v)$ decreases from 1 to 0.3 within two weeks, resulting in a 70% effectiveness for COVID-19 vaccines. This level of effectiveness persists for six months and then steadily wanes, reaching 0% (i.e., $1 - \sigma = 0$) after a year. This assumption is based on the administration of annual boosters, indicating that the COVID-19 vaccines' protection wanes after a year. The graph of $\sigma(a_v)$ is shown in Figure 16.

The vaccination rate $\nu(t)$ (see Figure 16) is fitted using the daily vaccination data for New York State (https://health.data.ny.gov/Health/New-York-State-Statewide-COVID-19-Vaccination-Data/duk7-xrni). It takes the form

$$\nu(t) = \begin{cases} 0 & \text{if } t \le 65, \\ 6 \times 10^{-5}(t - 65) & \text{if } 65 < t \le 110, \\ 0.27\% & \text{if } 110 < t \le 145, \\ 0.82\% & \text{if } 145 < t \le 200, \\ 0.50\% & \text{if } 200 < t \le 242, \\ 0.33\% & \text{if } t > 242. \end{cases}$$

We assume a vaccination rate of 0 before $t = 65$, aligning with the actual start of complete vaccinations (i.e., two-dose vaccination) in New York State on December 15, 2020. The rising vaccination rate from $t = 65$ to $t = 110$ reflects the initial scarcity of vaccine doses, which were prioritized for older adults and high-risk hospital workers. As vaccine production ramped up and more vaccination sites were established, the pace of vaccinations increased, making an increasing vaccination rate. After $t = 110$ we assume a series of distinct constant vaccination rates, each applicable to specific time intervals, to best represent the varying pace of vaccination during those periods. These constant rates for each interval have been determined based on data fitting.

We employ the Forward Euler Scheme with a time step of 0.1 to discretize our model using the parameter values mentioned above. The resulting graph depicting the daily and cumulative infections is represented by the red curves in Figure 14. It agrees well with the data, and our simulated curve aptly captures the significant surge in COVID-19 cases attributed to the Omicron variant.

We analyze the effects of p on the number of infectives in the model. The parameter p represents the number of days during which the infectious and symptomatic periods overlap. We explore two scenarios: $p = 1$, where the infectious period precedes symptoms by a day, and $p = 0$, where the infectious period and the symptomatic period coincide (see segments 3 and 4 in Figure 13). With other parameters held constant, the results for daily new and cumulative infectious cases are illustrated in Figures 18 and 19. Notably, for $p = 0, 1$, daily new cases near zero after 50 days, indicating effective disease control. This underscores the efficacy of hospitalizing symptomatic patients as a means to isolate infectious individuals and control the disease's progression.

Preprints (www.preprints.org) | NOT PEER-REVIEWED | Posted: 27 November 2023 doi:10.20944/preprints202311.1686.v1

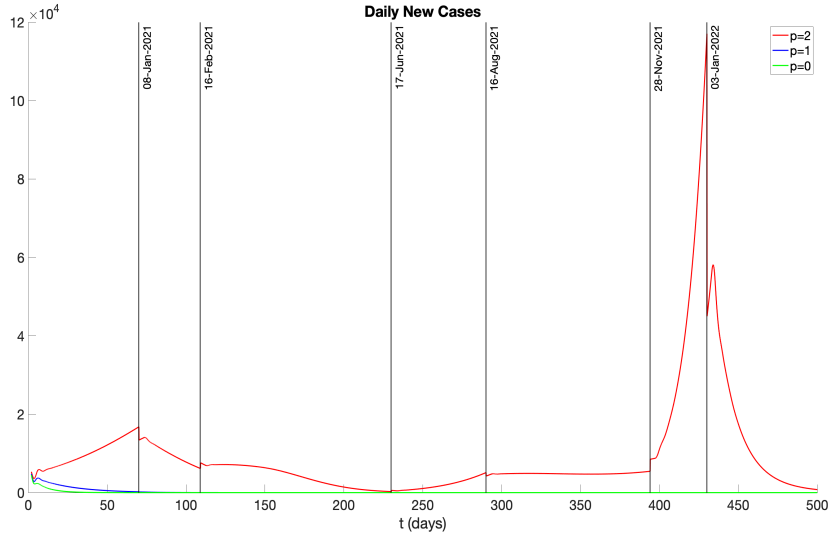

Figure 18. Daily new infectious cases represented by different curves for p values of 2, 1, and 0. Here, p denotes the overlap in days between infectious and symptomatic periods.

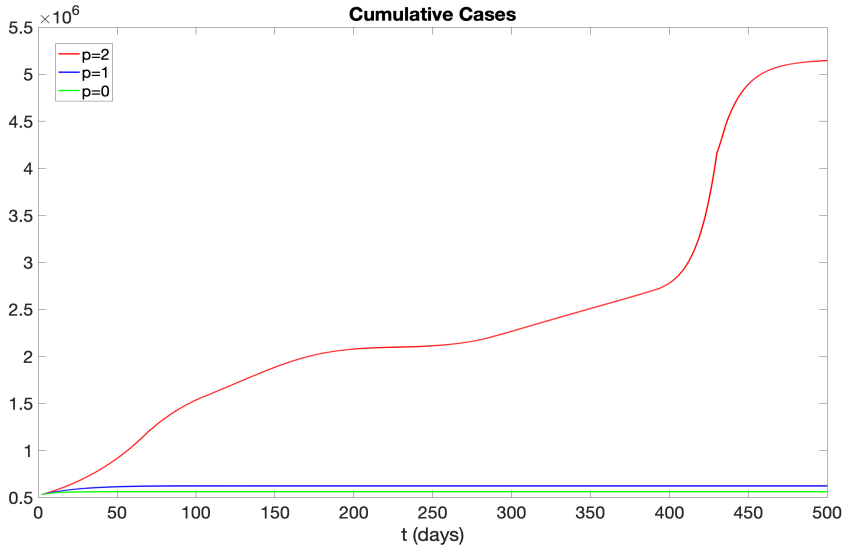

Figure 19. Cumulative infectious cases represented by different curves for p values of 2, 1, and 0. Here, p denotes the overlap in days between infectious and symptomatic periods.

In addition, we further examine the effects of varying vaccination rates on the number of infectives. Specifically, we consider two scenarios: one with a vaccination rate of $0.5\nu(t)$ and another with $2\nu(t)$. Figures 20 and 21 display the daily new and cumulative infectious cases for vaccination rates of $\nu(t)$, $0.5\nu(t)$, and $2\nu(t)$. Our findings suggest that a lower vaccination rate results in a higher number of infectious cases. Moreover, if the vaccination rate is doubled in the initial stage, the disease can be fully suppressed by approximately day 200. Another noteworthy observation is that with a vaccination rate of $0.5\nu(t)$, there is a peak in daily new infections around day 300. Yet, during the phase attributed to the Omicron variant, the number of new infections is significantly lower. This can be attributed to our assumption that infectives are not susceptible to re-infection. Consequently, the peak of infections around day 300 significantly reduces the number of susceptible individuals, and thus there are not many new infectious cases after day 400.

Preprints (www.preprints.org) | NOT PEER-REVIEWED | Posted: 27 November 2023 doi:10.20944/preprints202311.1686.v1

Building on our analysis of vaccination rates, we next turn our attention to the role of hospitalization rates in controlling the spread of COVID-19. We investigate how variations in the hospitalization rate (after symptoms appear), denoted by β_H, affect the number of infections. In Figure 22, we present the daily new cases, and in Figure 23, we illustrate the cumulative cases, each for a range of values from 0.51 to 0.58. The different curves in these figures demonstrate the sensitivity of the infection dynamics to hospitalization practices, revealing that higher hospitalization rates can significantly flatten the curve and reduce the total number of infections over time. These insights point to the critical impact of hospitalization rates on the management of the disease, alongside vaccination strategies.

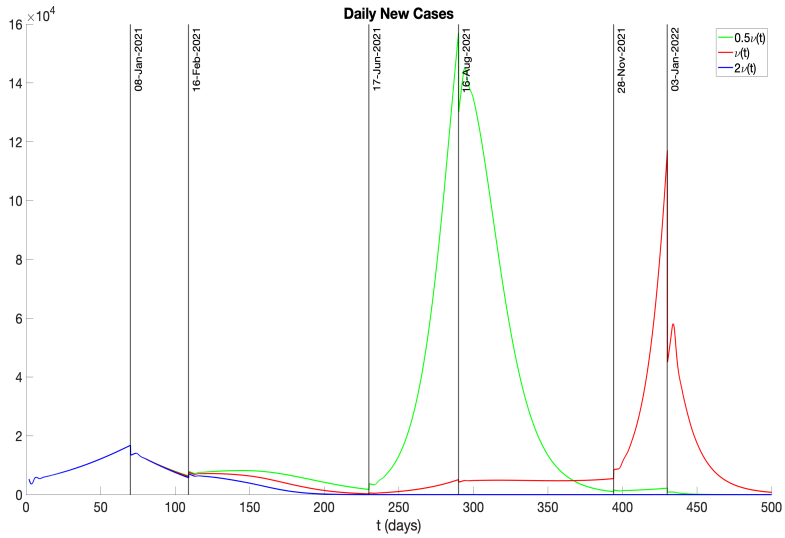

Figure 20. Daily new infectious cases with different vaccination rates $\nu(t)$, $2\nu(t)$, and $0.5\nu(t)$.

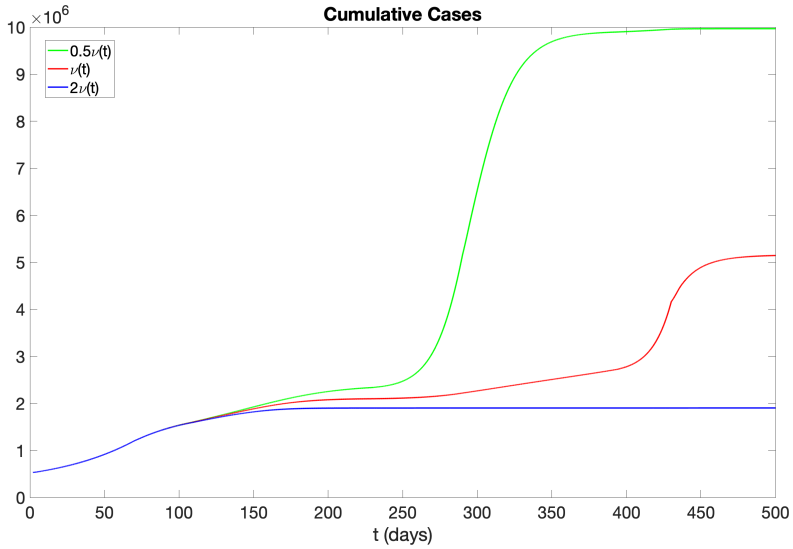

Figure 21. Cumulative infectious cases with different vaccination rates $\nu(t)$, $2\nu(t)$, and $0.5\nu(t)$.

Preprints (www.preprints.org) | NOT PEER-REVIEWED | Posted: 27 November 2023 doi:10.20944/preprints202311.1686.v1

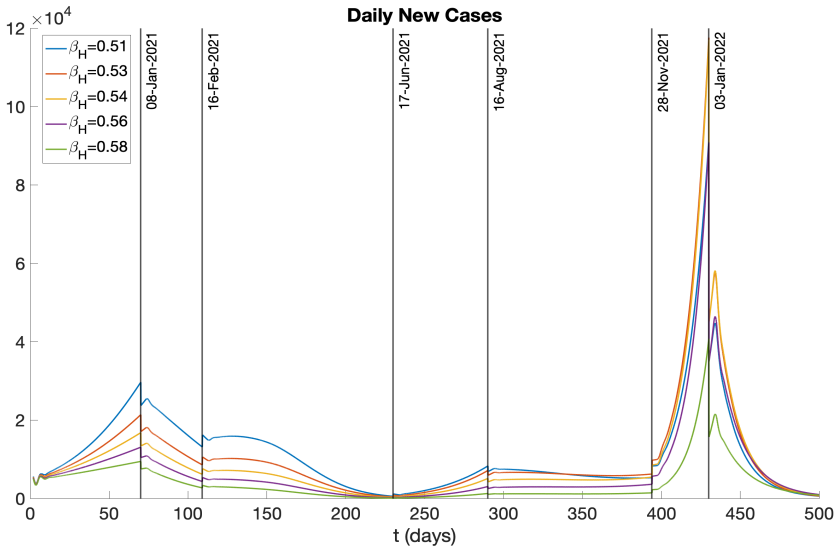

Figure 22. Daily new infectious cases represented by different curves for different β_H values.

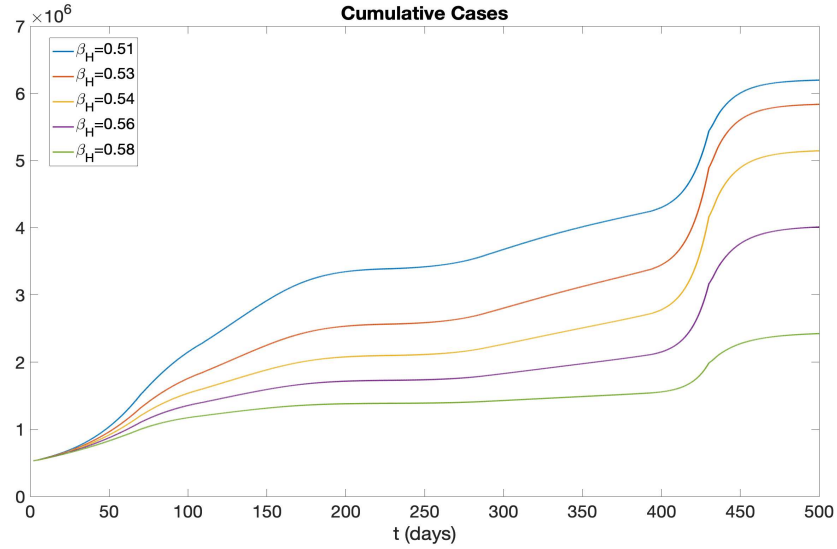

Figure 23. Cumulative infectious cases represented by different curves for different β_H values.

3. Conclusions

We have developed a population model of an epidemic structured by infection age and vaccination age. The population dynamics are analyzed with respect to infection age of infected individuals before symptoms appear, the fraction of pre-symptomatici infected individuals placed in quarantine, and the vaccine efficacy of vaccinated individuals with respect to their vaccination age. the model is applied to the 2003 SARS epidemic in Taiwan and the current COVID-19 epidemic in New York State. The computer codes for our numerical simulations are available upon request in both MATHEMATICA and MatLab.

In the application of the model to the 2003 SARS epidemic in Taiwan, in which vaccination was not available, the on-set of symptoms and the beginning of the infectious period coincided. The quarantine rate of susceptibles was approximately 2% per day. The epidemic was contained with the maximum cumulative number of infecteds at approximately 230 in 100 days (Figure 1).

We modified the pre-symptomatic and infectious periods to $p = 1$ and $p = 2$ days infectious pre-symptomatic. we also modified the quarantine rate to 4% and 10%. The results are shown in

 doi:10.20944/preprints202311.1686.v1

Figures 7–9, where it is seen that the value $p = 2$ has much higher cumulative cases than the value $p = 1$. When $p = 2$, the quarantine rate must be very high to significantly reduce the cumulative number of cases.

We also modified the 2003 SARS epidemic model to illustrate the impact of vaccination. In Figure 10 it is seen that infectious 2 days pre-symptomatic ($p = 2$), quarantine rate 4%, and the vaccine efficacy $\sigma(a_v) = .7\exp(-.25a_v) + .3$, results in a reduction of the maximum cumulative number of cases to 175,000 compared to 350,000 without vaccination.

In the application of the model to the current COVID-19 epidemic in New York State, the infectious period is pre-symptomatic by $p = 2$ days. This pre-symptomatic infectious period is a key feature of COVID-19 epidemic dynamics. From data sources, we parameterized the model into seven phases corresponding to vaccine implementation, viral variants, and social responses. The model simulations agree with the observed infection and vaccination (Figures 14 and 15).

We examined the consequences of modifying the pre-symptomatic infectious period, initially set at $p = 2$ days, by considering $p = 1$ day and $p = 0$ days. Figures 18 and 19 display numerical simulations for $p = 0, 1, 2$. It is seen that $p = 0$ and $p = 1$ result in a major reduction of the epidemic impact. We also investigated the impact of varying the vaccination rate parameter $\nu(t)$. Figures 20 and 21 show that an increase in $\nu(t)$ significantly mitigates the epidemic, while a decrease in $\nu(t)$ exacerbates the epidemic. Furthermore, we explored the effects of changing the hospitalization parameter $\beta_H(a_i)$. In Figures 22 and 23, we observed that higher values of $\beta_H(a_i)$ significantly decrease the epidemic's severity, whereas lower values of $\beta_H(a_i)$ increase the epidemic's severity.

In general, incorporating infection age and vaccination age into our analysis enables a detailed examination of key factors affecting epidemic outcomes. The continuum formulation of the infection age and vaccination age provides applicable parameter identification and numerical simulation of this age structure. Specifically, infection age and vaccination age can be connected to critical elements, such as pre-symptomatic infectiousness, vaccination efficacy, and hospitalization rate, which are integral to understanding and predicting epidemic dynamics.

While our model incorporates various factors, it remains a simplified representation of real-world disease transmission. It's important to highlight potential areas for refinement to make the model more realistic. For instance, reinfections are notably common with COVID-19 [14]. As the Omicron variant became predominant, data indicated a significant rise in reinfection rates among all COVID-19 cases [15]. Additionally, revaccination is another factor to account for, given the CDC's recommendation for individuals aged 12 and older to receive an updated COVID-19 vaccine annually [16]. A refined flow diagram that provides a more realistic depiction of disease transmission is presented in Figure 24. This diagram incorporates transitions such as $R \to S$, $Q \to S$, and $H \to S$ to account for reinfection, as well as the $V \to S$ transition for revaccination. We will consider models for this enhanced flow diagram in our future study. Notably, another promising direction for enhancement is the integration of chronological age. Data on COVID-19 often categorizes by age groups, and different age brackets might exhibit varied transmission rates [17–19]. This consideration will be a focus in our subsequent analyses.

 doi:10.20944/preprints202311.1686.v1

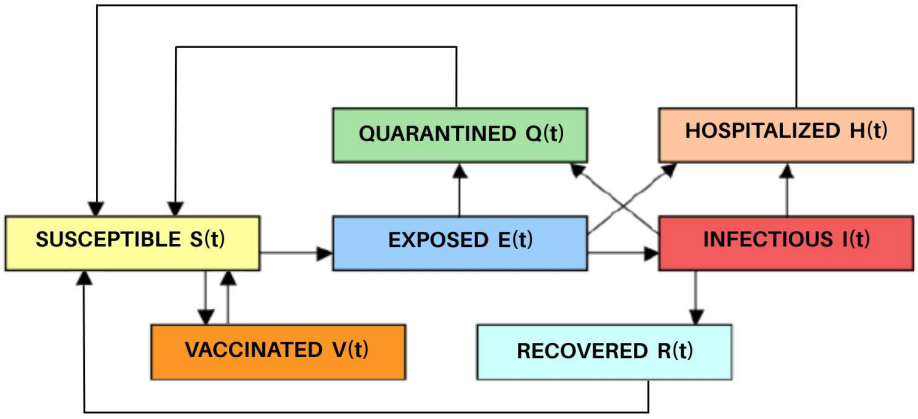

Figure 24. Diagram of susceptible, vaccinated, exposed, infectious, hospitalized, quarantined, and recovered compartments of a more realistic model.

Institutional Review Board Statement: Not applicable.

Informed Consent Statement: Not applicable.

Data Availability Statement: Not applicable.

Conflicts of Interest: The author declares no conflict of interest.

References

1. Sinestrari, E.; Webb, G. Nonlinear hyperbolic systems with nonlocal boundary conditions. *J. Math. Anal. Appl.*, **1987**, 121:449–464. doi.org/10.1016/0022-247X(87)90255-1.
2. Farkas, J. Stability conditions for the non-linear McKendrick equations. *Appl. Math. Comp.* **2004**, 156 (3),771-777. doi.org/10.1016/j.omc.2003.06.019.
3. Demongeot, J.; Griette, Q.; Maday, Y.; Magal, P. A Kermack?McKendrick model with age of infection starting from a single or multiple cohorts of infected patients. *Proc. R. Soc. A* **2023**, 479: 2022038120220381. doi.org/10.1098/rspa.2022.0381.
4. Hsieh, Y-H,; Chen, C,; Hsu, S-B. SARS Outbreak, Taiwan, 2003. *Emer. Inf. Dis.*, **2003**, 10(2):201-206. doi: 10.3201/eid1002.030515.
5. Hsieh, Y-H,; King, C-C; Chen, C,; Ho, M-S.; Hsu, S-B,; Wu, Y-C. Impact of quarantine on the 2003 SARS Outbreak: A retrospective modeling study. *J. Theoret. Biol.*, **2007**, 10(2):201-206. doi.10:1016/jtb.2006.09.015.
6. Webb, G.; Blazer, M.; Zhu, H.; Ardal S.; Wu, J. Critical role of nonsocomial transmission in the Toronto SARS outbreak. *Math. Bios. Eng.* **2004**, 1(1), 1-13, doi.10.3934/mbe.2004.1.1.
7. Webb, G.; Hsieh, Y-H.; Wu, J.; Blaser, M. Pre-symptomatic influenza transmission, surveillance, and school closings: Implications for novel influenza A (H1N1). *Math. Mod. Nat. Phen.* **2010**, 5(3), doi:10.1051/mmnp/20105312.
8. Kermack, W.; McKendrick, A. A contribution to the mathematical theory of epidemics. *Proc. Roy. Soc. Ser. A*, **1927**, 115(772):700–721. doi.org/10.1098/rspa.1927.0118.
9. Wikipedia, Compartmental Models in Epidemiology, 2023. https://en.wikipedia.org/wiki/Compartmental_models_in_epidemiology.
10. Wikipedia. Sars-cov-2 alpha variant, 2023. [Online; accessed 15-Octorber-2023].
11. Wikipedia. Sars-cov-2 delta variant, 2023. [Online; accessed 15-Octorber-2023].
12. Yale Medicine. Omicron, delta, alpha, and more: What to know about the coronavirus variants, 2023. [Online;September 1,2023].
13. Wikipedia. Sars-cov-2 omicron variant, 2023. [Online; accessed 15-Octorber-2023].

14. Centers for Disease Control and Prevention. What is covid-19 reinfection?, 2023. [Online; accessed 3-November-2023].
15. Ma. K. Trends in laboratory-confirmed SARS-CoV-2 reinfections and associated hospitalizations and deaths among adults aged >= 18 years 18 US jurisdictions, September 2021–December 2022. *MMWR. Morbidity and Mortality Weekly Report*, 72, 2023.
16. Centers for Disease Control and Prevention. Stay up to date with COVID-19 vaccines, 2023. [Online; accessed 3-November-2023].
17. Ram, R.; Schaposnik, L-P. A modified age-structured SIR model for COVID-19 type viruses. *Sci. Rep.*, **2021**, 11(1):15194. doi.org/10.1038/s41598-021-94609-3.
18. Calafiore, G-C.; Fracastoro, G. Age structure in SIRD models for the COVID-19 pandemic - A case study on Italy data and effects on mortality. *PloS ONE*, **2022**, 17(2):e0264324. doi.org/10.1371/journal.pone.0264324.
19. Luebben, G.; González-Parra, G.; Cervantes, B. Study of optimal vaccination strategies for earlyCOVID -19 pandemic using an age-structured mathematical model: A case study of the USA. *Math.Biosci. Eng.*, **2023** 20(6),10828–10865. 10.3934/mbe.2023481.
20. Aldila, D.; Samiadji, B.; Simorangkir, G.; Khosnaw, S.; Shahzad, M. Impact of early detection and vaccination strategy in COVID-19 eradication program in Jakarta, Indonesia. *Bmc Res. Notes* **2021**, *14, 132. doi.org/10.1186/s13104-021-05540-9.*
21. *Andrews, M; Bausch, C. Parameterizing a dynamic influenza model using longitudinal versus age-stratified case notifications yields different predictions of vaccine impacts.* Math. Biosci. Eng. **2019**, *16, 5, 3753-3770. doi: 10.3934/mbe.2019186.*
22. *Angulo, M.; Castanos, F.; Moreno-Morton, R.; Velasco-Hernandez, J.; Moreno, J. A simple criterion to design optimal non-pharmaceutical interventions for mitigating epidemic outbreaks.* Roy. Soc. Int. **2021**, *18, 20200803. doi.org/10.1098/rsif.2020.0803.*
23. *Arino, J.; Portet, S. A simple model for COVID-19.* Infect. Dis. Model. **2021**, *5, 309–315. doi.org/10.1016/j.idm.2020.04.002.*
24. *Ayoub, H.; Chemaitelly, H.; Mikhail, M.; Kanaani, Z.; Kuwari, E.; Butt, A.; Coyle, P.; Jeremijenko, A.; Kaleeckal, A.; Latif, A.; Shaik, R.; Rahim, H.; Nasrallah, G.; Yassine, H.; Kuwari, M.; Romaihi, H.; Al–Thani, M.; Bertollin, R.; Khai, A.; Abu–Raddad, L Epidemiological impact of prioritising SARS-CoV-2 vaccination by antibody status: mathematical modelling analyses.* BMJ Innov. **2021**, *7–327–336. doi: 10.1136/bmjinnov-2021-000677.*
25. *Betti, M.; Hefferman, J. A simple model for fitting mild, severe, and known cases during an epidemic with an application to the current SARS-CoV-2 pandemic.* Infect. Dis. Model. **2021**, 5,313–323. doi.org/10.1016/j.idm.2021.01.002.
26. Bonanca, P.; Angelillo, I.; Villani, A.; Biasci, P.; Scotti, S.; Russo, R.; Maio, T.; Rosati, G.; Barretta, M.; Bozzola, E.; Castiglia, P.; Chiamenti, G.; Conforti, G.; Conversano, M.; Ferro, A.; Francia, F.; Azzari, C. Maintain and increase vaccination coverage in children, adolescents, adults and elderly people: Let's avoid adding epidemics to the pandemic: Appeal from the Board of the Vaccination Calendar for Life in Italy: Maintain and increase coverage also by re-organizing vaccination services and reassuring the population. *Vaccine* **2021**, 39,1187-1189. doi.org/10.1016/j.vaccine.2020.10.024.
27. Bracis, C.; Burns, E.; Moore, M; Swan, D.; Reeves, D.; Schiffer, J.; Dimitrov, D. Widespread testing, case isolation and contact tracing may allow safe school reopening with continued moderate physical distancing: A modeling analysis of King County, WA data. *Infect. Dis. Model.* **2021**, 6,24–35. doi.org/10.1016/j.idm.2020.11.003.
28. Britton, T.; Ball, F.; Trapman, P. A mathematical model reveals the influence of population heterogeneity on herd immunity to SARS-CoV-2. *Science* **2020**, 369, 846–849, doi: 10.1126/science.abc6810.
29. Bubar, K.; Reinholt, K.; Kessler, S.; Lipsitch, M.; Cobey, S.; Grad, Y.; Larremore, D. Model-informed COVID-19 vaccine prioritization strategies by age and serostatus. *Science* **2021**, 371,916–921. doi: 10.1126/science.abe6959.
30. Byambasuren, O.; Cardona, M.; Bell, K.; Clark, J.; McLaws, M-L.; Glasziou, P. Estimating the extent of asymptomatic COVID-19 and its potential for community transmission: Systematic review and meta-analysis. *Off. J. Assoc. Med. Microbiol. Infect. Dis. Can.* **2020**, 5, 223–234. doi: 10.3138/jammi-2020-0030.
31. Byrne, A.; McEvoy, D.; Collins, A.; Hunt, K.; Casey, M.; Barber, A.; Butler, F.; Griffin, J.; Lane, E.; McAloon, C.; O'Brien, K.; Wall, P.; Walsh, K.; More, S. Inferred duration of infectious period of SARS-CoV-2: Rapid scoping review and analysis of available evidence for asymptomatic and symptomatic COVID-19 cases.Inferred duration of infectious period of SARS-CoV-2: Rapid scoping review and analysis of available

evidence for asymptomatic and symptomatic COVID-19 cases. *BMJ Open* **2020**, 10,e039856. doi:10.1136/bmjopen-2020-039856.

32. Cai, J; Deng, X.; Yang, J.; Sun, K.; Liu, H.; Chen, Z.; Peng, C.; Chen, X.; Wu, Q.; Zou, J.; Sun, R.; Zheng, W.; Zhao, Z.; Lu, W.; Liang, Y.; Zhou, X.; Ajelli, M.; Yu, H. Modeling transmission of SARS-CoV-2 Omicron in China. *Nature Medicine* **2022**, 28,1468?1475. doi.org/10.1038/s41591-022-01855-7.
33. Caldwell, J; Le, X.; McIntosh, L.; Meehan, M.; Ogunlade, S.; Ragonnet, R.; O'Neill, G.; Trauer, J.; McBryde, E. Vaccines and variants: Modelling insights into emerging issues in COVID-19 epidemiology. *Paediatric Resp. Rev.* **2021**, 39,32–39. doi.org/10.1016/j.prrv.2021.07.002.
34. Carlsson R.; Childs, L.; Feng, Z.; Glasser, J.; Heffernan, J.; Li, J.; Rost, G. Modeling the waning and boosting of immunity from infection or vaccination. *J. Theoret. Biol.* **2020**, 497,110265. doi.org/10.1016/j.jtbi.2020.110265
35. Choi, Y.; Kim, J.; Kim, J.E.; Choi, H.; Lee, C. Vaccination prioritization strategies for COVID-19 in Korea: A mathematical modeling approach. *Int. J. Environ. Res. P. H.* **2021**, 18,4240. doi.org/10.3390/ijerph18084240.
36. Contreras, S.; Priesemann, V. Risking further COVID-19 waves despite vaccination. *Lancet Infect. Dis.* **2021**, 21,6,745–746. doi:10.1016/S1473-3099(21)00167-5.
37. Das, P.; Upadhyay, R.; Misra, A.; Rihan, F.; Das, P.; Ghosh, D. Mathematical model of COVID-19 with comorbidity and controlling using non-pharmaceutical interventions and vaccination. *Nonl. Dyn.* **2021**, 106(2):1213–1227. doi:10.1007/s11071-021-06517-w.
38. Dashtbali, M.; Mirzaie, M. A compartmental model that predicts the effect of social distancing and vaccination on controlling COVID-19. *Sci. Rep. UK* **2021**, 11,8191, doi.org/10.1038/s41598-021-86873-0.
39. Dean, N.; Pastore, Y.; Piontti, A.; Madewell, Z.; Cummings, D.; Hitchings, M.; Joshi, K.; Kahn, R.; Vespignani, A.; Halloran, M.; Longini, I. Ensemble forecast modeling for the design of COVID-19 vaccine efficacy trials. *Vaccine* **2020**, 38,7213–7216, doi.org/10.1016/j.vaccine.2020.09.031.
40. De la Sen, M.; Ibeas, A. On an SE(Is)(Ih)AR epidemic model with combined vaccination and antiviral controls for COVID-19 pandemic. *Adv. Dif. Eq.* **2021**, 2021(1):92. doi:10.1186/s13662-021-03248-5.
41. Demongeot, J.; Griette, Q.; Magal, P. SI epidemic model applied to COVID-19 data in mainland China. *Roy. Soc. Open Sci.* **2021**, 7,21878. doi.org/10.1098/rsos.201878.
42. Demongeot, J.; Griette, Q.; Magal, P.; Webb, G. Modeling vaccine efficacy for COVID-19 outbreak in New York City. *Biology* **2022**, 11,345. doi.org/10.3390/biology11030345.
43. Duan, X.; Yuan, S.; Li, X. Global stability of an SVIR model with age of vaccination. *Appl. Math. Comp.* **2014**, 226,1, 528-540. doi.org/10.1016/j.amc.2013.10.073.
44. Duan, X.; Yuan, S.; Qiu, Z; Ma, J. Global Stability of an SVEIR epidemic model with ages of vaccination and latency. *Comp. Math. Appl.* **2014**, 68,268-309. doi.org/10.1016/j.camwa.2014.06.002.
45. Eikenberry, S.; Muncuso, M.; Iboi, E.; Phan, T.; Eikenberry, K.; Kuang, Y.; Kostelich, E.; Gummel, A. To mask or not to mask: Modeling the potential for face mask use by the general public to curtail the COVID-19 pandemic. *Infect. Dis. Model.* **2021**, 5,293–308. doi.org/10.1016/j.idm.2020.04.001.
46. Elhia, M.; Chokri, K.; Alkama, M. Optimal control and free optimal time problem for a COVID-19 model with saturated vaccination function. *Commun. Math. Biol. Neurosci.* **2021**, 35. doi:10.28919/cmbn/5632.
47. Firth, J.; Hellewell, J.; P. Klepac, P.; Kissler, S.; CMMID COVID-19 Working Group; Kucharski, A.; Spurgin, L. Using a real-world network to model localized covid-19 control strategies. *Nat. Med* **2020**, 26,1616–1622. doi.org/10.1038/s41591-020-1036-8.
48. Fontanet , A.; Cauchemez, S. COVID-19 herd immunity: where are we? *Nat. Rev. Immunol.* **2020**, 20,583–584, doi.org/10.1038/s41577-020-00451-5.
49. Forien, R.; Pang, G.; Pardoux, E. Estimating the state of the COVID-19 epidemic in France using a model with memory. *Roy. Soc. Open Sci.* **2021**, 8(3):202327. doi:10.1098/rsos.202327.
50. Foy, B.; Wahl, B.; Mehta, K.; Shet, A.; Menon, G.; Britto, C. Comparing COVID-19 vaccine allocation strategies in India: A mathematical modelling study. *Int. J. Infect. Dis.* **2021**, 103,431–438. doi.org/10.1016/j.ijid.2020.12.075.
51. Ghosh, S.; Ghosh, S. A mathematical model for COVID-19 considering waning immunity, vaccination and control measures. *Sci. Rep.* **2023**, 13,3610. doi.org/10.1038/s41598-023-30800-y.
52. Giordano, G.; Colaneri, M.; Di Filippo, A.; Bianchini, F.; Bolzern, P.; Nicolao, G.; Sacchi, P.; Colaneri, P.; Bruno, R. Modeling vaccination rollouts, SARS-CoV-2 variants and the requirement for non-pharmaceutical interventions in Italy. *Nat. Med.* **2021**, 27,993?998. doi.org/10.1038/s41591-021-01334-5.

53. Gokbulut, N.; Kuymakamzade, B.; Sanlidag, T.; Hincal, E. Mathematical modelling of Covid-19 with the effect of vaccine. *Aip Conf. Proc.* **2021**, *2325*, 020065. doi:10.1063/5.0040301.
54. Goldstein, Cassidy, T.; Wachter, K. Vaccinating the oldest against COVID-19 saves both the most lives and most years of life. *Proc. Natl. Acad. Sci. USA* **2021**, 118 (11) e2026322118. doi:10.1073/pnas.2026322118.
55. Griette, Q.; Magal, P. Clarifying predictions for COVID-19 from testing data: the example of New-York State. *Infect. Dis. Model.*, **2021**, 6,273–283. doi.org/10.1016/j.idm.2020.12.011.
56. Griette, Q.; Liu, Z.; Magal, P.; Thompson, R. Real-time prediction of the end of an epidemic wave: COVID-19 in China as a case-study. *Mathematics of Public Health. Fields Institute Communications, Vol 85*, **2020**, doi.org/10.1007/978-3-030-85053-18.
57. Gumel, A.; Ibio, E.; Ngonghala, C.; Elbas, E. A primer on using mathematics to understand COVID-19 dynamics: Modeling, analysis and simulations. *Infect. Dis. Model.* **2021**, 6,148-168. doi.org/10.1016j.idm.2020.11.005.
58. Hellewell, J.; Abbott, S.; Gimma, A.; Bosse, N.; Jarvis, C.; Russell, T.; Munday, J.; Kucharski, A.; Edmunds, W. Feasibility of controlling COVID-19 outbreaks by isolation of cases and contacts. *Lancet Glob. Health* **2020**, 8,E488–E496. doi.org/10.1016/S2214-109X(20)30074-7.
59. Huo, X.; Chen, J.; Ruan, S. Estimating asymptomatic, undetected and total cases for the COVID-19 outbreak in Wuhan: a mathematical modeling study. *Bmc Infect Dis.* **2021**, 21(10:476. doi:10.1186/s12879-021-06078-8.
60. Huo, X.; Sun, X.; Bragazzi, N.; Wu, J. Effectiveness and feasibility of convalescent blood transfusion to reduce COVID-19 fatality ratio. *Roy. Soc. Open Sci.* **2021**, 8:202248. doi:10.1098/rsos.202248.
61. Iboi, E.; Ngonghala, C.; Gumel, A. Will an imperfect vaccine curtail the COVID-19 pandemic in the US? *Infect. Dis. Model.* **2021**, 5,510–524. doi.org/10.1016/j.idm.2020.07.006.
62. IHME COVID-19 Forecasting Team; Modeling COVID-19 scenarios for the United States. *Nat Med.* **2021**, 27,94–105. doi.org/10.1038/s41591-020-1132-9.
63. Inayaturohmat, F.; Zikkah, R.; Supriatna, A.; Anggriani, N. Mathematical model of COVID-19 transmission in the presence of waning immunity. *J. Phys. Conf. Ser.* **2021**, *1722*, 012038. doi.org/10.1088/1742-6596/1722/1/012038.
64. Jackson, L.; Anderson, E.; Rouphael, N. An mRNA Vaccine against SARS-CoV-2 - Preliminary Report. *New Engl. J. Med.* **2021**, 383,1920–1931. doi: 10.1056/NEJMoa2022483.
65. Jentsch, P.; Anand, M.; Bauch, C. Prioritising COVID-19 vaccination in changing social and epidemiological landscapes: A mathematical modelling study. *Lancet Infect. Dis.* **2021**, 8:1097-1106. doi:10.1016/S1473-3099(21)00057-8.
66. Jewell, N.; Lewnard, J.; Jewell, B. Predictive mathematical models of the COVID-19 pandemic: Underlying principles and value of projections. *JAMA*, **2020**, 323,1893–1894. doi:10.1001/jama.2020.6585.
67. Johansson, M.; Quandelacy, T.; Kada, S.; Prasad, P.; Steele, M.; Brooks, J.; Slayton, R.; Biggerstaff, M.; Butler, J. SARS-CoV-2 Transmission From People Without COVID-19 Symptoms. *JAMA Netw. Open* **2021**, 4(1):e2035057. doi:10.1001/jamanetworkopen. 2020.35057.
68. Johnston, M.; Pell, B.; Nelson, P. A mathematical study of COVID-19 spread by vaccination status in Virginia. *Appl. Sci.* **2022**, 12,1723. doi.org/10.3390/app12031723.
69. Kalyan, D.; Kumar, G.; Reddy K.; Lakshminarayand, K. Sensitivity and elasticity analysis of novel corona virus transmission model: A mathematical approach. *Sensors Int.* **2021**, 2,100088, doi.org/10.1016/j.sintl.2021.100088.
70. Keeling, M.; Hill, E.; Gorsich, E.; Penman, B.; Guyver-Fletcher, G.; Holmes, A.; Leng, T.; McKimm, H.; Tamborrino, M.; Dyson, L.; Tildesley, M. Predictions of COVID-19 dynamics in the UK: Short-term forecasting and analysis of potential exit strategies. *PLoS Comput. Biol.* **2021**, 17(1): e1008619. doi:10.1371/journal.pcbi.1008619.
71. Krueger, T,; Gogolewski, K.; Bodych, M., Gambin, A.,; Giordano,G.; Cuschieri, S.; Czypionka, T,; Perc, M.; Petelos,E.; Rosinska, M.; Szczurek, E. Risk assessment of COVID-19 epidemic resurgence in relation to SARS-CoV-2 variants and vaccination passes. *Comm. Med.(Lond)* **2022**, 2, 23. doi.org/10.1038/s43856-022-00084-w.
72. Kucharski, A.; Russell, T.; Diamond, C.; Liu, Y.; Edmunds, J.; Funk, S.; Eggo, R. Early dynamics of transmission and control of covid-19: A mathematical modelling study. *Lancet Infect. Dis.* **2020**, *20*, 553–558, doi.org/10.1016/S1473-3099(20)30144-4.

73. Lauer, S.; Grantz K.; Bi, Q.; Jones, F.; Zheng, Q.; Meredith, H.; Azman, A.; Reich, N.; Lesser, J. The incubation period of coronavirus disease 2019 (COVID-19) from publicly reported confirmed cases: Estimation and application. *Ann. Intern. Med.* **2020**, 172,577–582. doi:10.7326/M20-0504external.
74. Libotte, G.; Lobato, F.; Platt, G.; Neto, A. Determination of an optimal control strategy for vaccine administration in COVID-19 pandemic treatment. *Comput. Meth. Prog. Biol.* **2020**, 196,105664. doi.org/10.1016/j.cmpb.2020.105664.
75. Lipsitch, M.; Dean, N. Understanding COVID-19 vaccine efficacy. *Science* **2020**, 370,763–765, doi: 10.1126/science.abe5938.
76. Liu, Z.; Magal, P.; Seydi, O.; Webb, G. Understanding unreported cases in the 2019 -n Cov epidemic outbreak in Wuhan, China, and the importance of major public health interventions. *Biology* **2020**, 9(3):50. doi:10.3390/biology9030050.
77. Liu, Z.; Magal, P.; Seydi, O.; Webb, G. A COVID-19 epidemic model with latency period. *Infect. Dis. Mod.* **2021**, 5,323–337. doi.org/10.1016/j.idm.2020.03.003.
78. Magal, P.; Webb, G. The parameter identification problem for SIR epidemic models: Identifying unreported cases. *J. Math. Biol.* **2018**, 77,1629–1648. doi.org/10.1007/s00285-017-1203-9.
79. Majeed, B.; David, J.; Bragazzi, N.; McCarthy, Z.; Grunnill, M.; Heffernan, J.; Wu, J.; Woldegerima, W. Mitigating co-circulation of seasonal influenza and COVID-19 pandemic in the presence of vaccination: A mathematical modeling approach. *Front. Pub. Health* **2023**, 10,1086849. doi.org/10.3389/fpubh.2022.1086849.
80. Makhoul, M.; Chemaitelly, H.; Ayoub, H.; Seedat, S.; Abu-Raddad, L. Epidemiological Differences in the Impact of COVID-19 Vaccination in the United States and China. *Vaccines* **2021**, 9,223. doi.org/10.3390/vaccines9030223.
81. Mancuso, M,; Eikenberry, S.; Gumel, A. Will vaccine-derived protective immunity curtail COVID-19 variants in the US? *Inf. Dis. Mod.* **2021**, 6,1110-1134. doi.org/10.1016/j.idm.2021.08.008.
82. Mandal, M.; Jana, S.; Nandi, S.; Khatua, A.; Adak, S.; Kar, T. A model based study on the dynamics of COVID-19: Prediction and control. *Chaos Soliton. Fract.* **2020**, 136,109889. doi.org/10.1016/j.chaos.2020.109889.
83. Martinez-Rodriguez, D.; Gonzalez-Parra, G.; Villanueva, R-J. Analysis of key factors of a SARS-CoV-2 vaccination program: A mathematical modeling approach. *Epidemiologia* **2021**, 2,140–161, doi:10.3390/epidemiologia2020012.
84. Matrajt, L.; Halloran, M.; Antia, M. Successes and failures of the live-attenuated influenza vaccine: Can we do better? *Clin. Infect. Dis.* **2020**, 70,1029–1037. doi.org/10.1093/cid/ciz358.
85. Matrajt, L.; Eaton, J.; Leung, T.; Brown, E. Vaccine optimization for COVID-19: Who to vaccinate first? *Sci. Adv.* **2020**, 7(6). doi: 10.1126/sciadv.abf1374.
86. McDonnell, A.; Van Exan, R.; Lloyd, S.; Subramanian, L.; Chalkidou, K.; La Porta, A.; Li, J.; Maiza, E.; Reader, D.; Rosenberg, J.; Scannell, J.; Thomas, V.; Weintraub, R.; Yadav, P. COVID-19 vaccine predictions: using mathematical modelling and expert opinions to estimate timelines and probabilities of success of COVID-19 vaccines. *Cent. Glob. Dev.* **2020**, CGD Policy Paper 183, October 2020. covid19.ariadnelabs.org.
87. Mizumoto, K.; Chowell, G. Transmission potential of the novel coronavirus (COVID-19) onboard the diamond Princess Cruises Ship, 2020. *Infect. Dis. Mod.* **2021** 5,264–270. doi.org/10.1016/j.idm.2020.02.003.
88. Moghadas, S.; Fitzpatrick, M.; Sah, P.; Pandey, A.; Shoukat, A.; Singer, B.; Galvani, A. The implications of silent transmissin for the control of COVID-19 outbreaks. *Proc. Natl. Acad. Sci. USA* **2020**, 117,17513–17515. doi.org/10.1073/pnas.2008373117.
89. Moore, S.; Hill, E.; Dyson, L.; Tildesley, M.; Keeling, M. Modelling optimal vaccination strategy for SARS-CoV-2 in the UK. *PLOS Comput. Biol.* **2021**, doi:10.1371/journal.pcbi.1008849.
90. Moore, S.; Hill, E.; Tildesley, M.; Dyson, L.; Keeling, M. Vaccination and non-pharmaceutical interventions for COVID-19: A mathematical modelling study. *Lancet Infect. Dis.* **2021**, 21(6):793-802. doi:10.1016/S1473-3099(21)00143-2.
91. Olivares, A.; Steffetti, E. Uncertainty quantification of a mathematical model of COVID-19 transmission dynamics with mass vaccination strategy. *Chaos Soliton. Fract.* **2021**, 146:110895. doi:10.1016/j.chaos.2021.110895.
92. Ng V.; Fazil, A.; Waddell, L.; Turgeon, P.; Otten, A.; Ogden, N. Modelling the impact of shutdowns on resurging SARS-CoV-2 transmission in Canada. *Roy. Soc. Open Sci.* **2021**, 8,5. doi:10.1098/rsos.210233.

93. Ngonghala, C.; Iboi, E.; Eikenberry, S.; Scotch, M.; MacIntyre, C.; Bonds, M.; Gumel, A. Mathematical assessment of the impact of non-pharmaceutical interventions on curtailing the 2019 novel coronavirus. *Math. Biosci.* **2020**, 9,108364. doi.org/10.1016/j.mbs.2020.108364.
94. Ngonghala, C.; Iboi, E.; Gumel, A. Could masks curtail the post-lockdown resurgence of covid-19 in the US? *Math. Biosci.* **2020**, 329,108452. doi.org/10.1016/j.mbs.2020.108452.
95. Ngonghala, C; Gumel, A. Mathematical assessment of the role of vaccination against COVID-19 in the United States. Mathematical Modelling, Simulations, and AI for Emergent Pandemic Diseases *Science Direct* **2023**, 221-249. doi.org/10.1016/B978-0-323-95064-0.00013-0.
96. Noh, J.; Danuser, G. Estimation of the fraction of COVID-19 infected people in U.S. states and countries worldwide. *PLoS ONE* **2021**, 16. doi:10.1371/journal. pone.0246772.
97. Paget, J.; Caini, S.; Cowling, B.; Esposito, S.; Falsey, A.; Gentile, A.; Kynci, J.; Macintyre, C.; Pitman, R.; Lina, B. The impact of influenza vaccination on the COVID-19 pandemic? Evidence and lessons for public health policies. *Vaccine* **2021**, 38,6485–6486. doi:10.1016/j.vaccine.2020.08.024.
98. Paltiel, A.; Schwartz, J.; Zheng, A.; Walensky, R. Clinical outcomes of a COVID-19 vaccine: Implementation over efficacy. *Health Aff.* **2021**, 40(1):42-52. doi:10.1377/hlthaff.2020.02054.
99. Peak, C.; Kahn, R.; Grad, H.; Childs, L.; Li, R.; Lipstich, M.; Buckee, C. Individual quarantine versus active monitoring of contacts for the mitigation of COVID-19: a modelling study. *Lancet Infect. Dis.* **2020**, 20,1025–1033. doi.org/10.1016/S1473-3099(20)30361-3.
100. Poonia, R.; Saudagar A.; Altameem, A.; Alkhathami, M.; Khan, M.; Hasanat, M. An enhanced SEIR model for prediction of COVID-19 with vaccination effect. *Life* **2022**, 12,647. doi.org/10.3390/life12050647.
101. Roosa, K.; Lee, Y.; Luo, R.; Kirpich, A.; Rothenberg, R.; Hyman, M.; Yan, P.; Chowell, G. Real-time forecasts of the COVID-19 epidemic in China from February 5th to February 24th, 2020. *Infect. Dis. Mod.* **2021**, 5,256–263. doi.org/10.1016/j.idm.2020.02.002.
102. Rosenberg, E.; Dorabawila, V.; Easton, D.; Bauer, U.; Kumar, J.; Hoen, R.; Hoefer, D.; Wu, M.; Lutterloh,E.; Conroy, M.; Greene, D.; Zucker, H. Covid-19 effectiveness in New York State. *N. Engl. J. Med.* **2022**, 86,116-127. doi: 10.1056/NEJMoa2116063.
103. Saldana, F.; Fiores-Arguedas, H.; Camacho-Gutierrez, J.; Barradas, I. Modeling the transmission dynamics and the impact of the control interventions for the COVID-19 epidemic outbreak. *Math. Biosci. Eng.* **2020**, 17,4165–4183. doi.org/10.3934/MBE.2020231.
104. Saldana, F.; Velasco-Hernandez, J. The trade-off between mobility and vaccination for COVID-19 control: A metapopulation modelling approach. *Roy. Soc. Open Sci.* **2021**, 8,202240. doi:10.1098/rsos.202240.
105. Shim, E.; Tariq, A.; Choi, W.; Lee, Y.; Chowell, G. Transmission potential and severity of COVID-19 in South Korea. *Int. J. Infect. Dis.* **2020**, 93,339–344. doi:10.1016/j.ijid.2020.03.031.
106. Shim, E. Optimal allocation of the limited COVID-19 vaccine supply in South Korea. *J. Clin. Med.* **2021**, 10,591. doi:10.3390/jcm10040591.
107. Sun, D.; Teng, Z.; Wang, K.; Zhang, T. Stability and Hopf bifurcation in delayed age-structured SVIR epidemic model with vaccination and incubation. *Chaos, Soliton. Fract.* **2023**, 168,113206. doi.org/10.1016/j.chaos,113206.
108. Sung-mok, J.; Akira, E.; Ryo, K.; Hiroshi, N. Projecting a second wave of COVID-19 in Japan with variable interventions in high-risk settings. *Roy. Soc. Open Sci.* **2021**, 8:202169. doi:10.1098/rsos.202169.
109. Tang, B.; Bragazzi, N.; Li, Q.; Tang, S.; Xiao, Y.; Wu, J. An updated estimation of the risk of transmission of the novel coronavirus (2019-nCov). *Infect. Dis. Mod.* **2021** 5,248–255. doi.org/10.1016/j.idm.2020.02.001.
110. Tang, B.; Zhang, X.; Li, Q.; Bragazzi, N.; Golemi-Kotra, D.; Wu, J. The minimal COVID-19 vaccination coverage and efficacy to compensate for a potential increase of transmission contacts, and increased transmission probability of the emerging strains. .*BMC Public Health* **2022**, 22,1258. doi.org/10.1186/s12889-022-13429-w.
111. Tang, J.; Jin, Z.; Wang, L.; Xu, F. A note on an age-of-infection SVIR model with nonlinear incidence. *Int. J. Biomath.* 10,05, 750064. doi.org/10.1142/S1793524517500644.
112. Tariq, A.; Lee, L.; Roosa, K.; Blumberg, S.; Yan, P.; Ma, S.; Chowell, G. Real-time monitoring the transmission potential of COVID-19 in Singapore. *BMC Med.* **2020**, 18,1–14. doi.org/10.1186/s12916-020-01615-9.
113. Troiano, G.; Nordi, A. Vaccine hesitancy in the era of COVID-19. *Public Health* **2021**, 194,245-251. doi.org/10.1016/j.puhe.2021.02.025.

114. Thunstrom, L.; Ashworth, M.; Newbold, S. Hesitancy towards a COVID-19 vaccine and prospects for herd immunity. *SSRN Elect. J.* **2020**, doi:10.2139/ssrn.3593098.
115. Thurmer, S.; Klimek, P.; Hanel, R. A network-based explanation of why most covid-19 infection curves are linear. *Proc. Natl. Acad. Sci. USA* **2020**, 17,22684–22689. doi.org/10.1073/pnas.2010398117.
116. Usherwood, T.; LaJoie, Z.; Srivastava, V. c. *Sci. Rep.* **2021**, 11(1):12051. doi:10.1038/s41598-021-91514-7.
117. Waku, J.; Oshinubi, K.; Adam, U.; Demongeot, J. Forecasting the endemic/epidemic transition in COVID-19 in some countries: Influence of the vaccination. *Nature* **2023** 11,135. doi.org/10.3390/diseases11040135.
118. Wang, J.; Zhang, R; Kuniya, I. The dynamics of an SVIR epidemiological model with infection age. *IMA J. Appl. Math.* **2016**, 81,2,321-343. doi.org/10.1093/imamat/hxv039.
119. Wang, J.; Lang, J.;Chen, Y. Global threshold dynamics of an SVIR model with age-dependent infection and relapse. *J. Biol. Dyn.* **2017**, 11,1850068. doi.org/10.1080/17513758.2016.1226436.
120. Wang, C..; Fan, D; Xia, L.; Yi, X. Global stability for a multi-group SIVR model with age of vaccination. *Int. J. Biomath.* **2018**, 11,05,1850068. doi.org/10.1142/S1793524518500687.
121. Wang, Z.; Muecksch, F.; Schaefer-Babajew, D.; Finkin, S.; Viant, C.; Gaebler, C.; Hoffman, H.; Barnes, C.; Cipolla, M.; Ramos, V.; Oliveira T.; Cho A.; Schmidt F.; Da Silva J.; Bednarski E.; Aguado L.; Yee J.; Daga M.; Turroja M.; Millard K.; Jankovic M.; Gazumyan A.; Zhao Z.; Rice C.; Bieniasz P.; Caskey M.; Hatziioannou T.; Nussenzweig M. Naturally enhanced neutralising breadth against SARS-CoV-2 one year after infection. *Nature* **2021**, 595(7867):426-431. doi:10.1038/s-41586-021-03696-9.
122. Wang, S.; Wu, Y.; Li, L.; Li, Y.; Sun, G. Forecast for peak infections in the second wave of the Omicron after the adjustment of zero-COVID policy in the mainland of China. *Infect. Dis. Rep.* **2023**, 8 562-573. doi.org/10.1016/j.idm.2023.05.007.
123. Webb, G. A COVID-19 epidemic model predicting the effectiveness of vaccination. *Math. Appl. Sci. Eng.* **2021**, 2(2):1-15. doi:10.5206/mase/13889.
124. Webb, G. A COVID-19 epidemic model predicting the effectiveness of vaccination in the US. *Infect. Dis. Rep.* **2021**, 13,654-657. doi.org/10.3390/idr13030062.
125. Wilder, B.; Champignon, M.; Killian, J.; Ou, H-C.; Mate, A.; Jabbari, S.; Perrault, A.; Desai, A.; Taube, M.; Majumder, M. Modelling between-population variation in COVID-19 dynamics in Hubei, Lombardy, and New York City. *Proc. Natl. Acad. Sci. USA* **2020**, 117,25904–25910. doi.org/10.1073/pnas.2010651117.
126. Xing, Y.; Li, H. Almost periodic solutions for a SVIR epidemic model with relapse. *Math. Bios. Eng.* **2021**, 18,6,7191-7217. doi.org/10.3934/mbe.202135634814245
127. Xue, L.; Jing, S.; Miller, J.; Sun, W.; Li, H.; Estrada-Franco, J.; Hyman, J.; Zhu, H. A data-driven network model for the emerging covid-19 epidemics in Wuhan, Toronto and Italy. *Math. Biosci.* **2020**, 326,108391. doi.org/10.1016/j.mbs.2020.108391.
128. Yang, J.; Yang, L.; Jin, Z. Optimal strategies of the age-specific vaccination and antiviral treatment against influenza. *Chaos Soliton. Fract.* **2023**, 68,113199. doi.org/10.1016/j.chaos.2023.113199.